

## Field dependence of the $^{19}\text{F}$ and $^{55}\text{Mn}$ nuclear spin-lattice relaxation in antiferromagnetic $\text{MnF}_2$ †

D. Paquette,\* A. R. King, and V. Jaccarino

Physics Department, University of California, Santa Barbara, California 93106

(Received 22 August 1973)

The  $^{19}\text{F}$  and  $^{55}\text{Mn}$  nuclear spin-lattice relaxation (NSLR) rates in  $\text{MnF}_2$  have been used to study the effects of an external magnetic field  $\vec{H}_0 \parallel \hat{c}$  on the magnetic excitations of a uniaxial antiferromagnet at temperatures  $T \ll T_N$ . In the region  $0 \leq H_0 < H_{\text{SF}}$ , the "spin-flop" field, a striking variation of both rates is observed. Except in the immediate vicinity of  $H_{\text{SF}}$ , quantitative agreement between experiment and theory is obtained for the two-magnon-induced  $^{19}\text{F}$  NSLR and three-magnon (exchange enhanced)  $^{55}\text{Mn}$  NSLR. The importance of pair correlation to the Raman scattering in the  $^{19}\text{F}$  NSLR is clearly demonstrated. Both the  $^{19}\text{F}$  and  $^{55}\text{Mn}$  NSLR rates exhibit a critically like divergent behavior as  $H_0$  approaches  $H_{\text{SF}}$  which is not explained by lower-order spin-wave scattering theory. In particular the  $^{55}\text{Mn}$  NSLR rate diverges as  $(H_{\text{SF}} - H_0)^{-3/2}$  in the immediate vicinity of  $H_{\text{SF}}$ . This property of the NSLR rate is consistent with the theory of a direct process in which the magnons are assumed to have a finite lifetime  $\Gamma_{\vec{k}}^{-1}$  and from which a value  $\Gamma_{\vec{k}} = 1.8 \times 10^6 \text{ sec}^{-1}$  is obtained, at  $T = 4.2^\circ\text{K}$  and  $H \approx H_{\text{SF}}$ . An effective-field theory of  $\chi_{\perp}$  vs  $\vec{H}_0 \parallel \hat{c}$  is developed and predicts an  $(H_{\text{SF}} - H_0)^{-1}$  divergence to both  $\chi_{\perp}$  and rf-field enhancements of the NMR in an antiferromagnet. A satisfactory comparison between the observed enhancements and this theory is obtained.

### I. INTRODUCTION

During the past two decades there have been numerous studies of the excitations of magnetically ordered spin systems. Using data obtained from a variety of both microscopic and macroscopic experimental techniques, detailed comparisons have been made with the predictions of spin-wave theories of varying degrees of sophistication. In a few simpler systems, where the spin interactions may be accurately characterized, considerable success was achieved with regard to the determination of the excitation spectra and the extent to which spin-wave interactions affect various thermodynamic properties. A summary of spin-wave theory and its application to the thermodynamics of magnetic systems has been given by Keffer.<sup>1</sup>

The uniaxial antiferromagnet  $\text{MnF}_2$  is one such spin lattice. Precise measurements have been obtained of the spin-wave dispersion,<sup>2</sup> the magnitude and temperature dependence of the parallel<sup>3,4</sup> and perpendicular<sup>3</sup> susceptibilities, the sublattice magnetization,<sup>4,5</sup> the magnetic specific heat,<sup>4,6</sup> and the antiferromagnetic resonance frequency<sup>7</sup> and linewidths.<sup>8</sup> The magnetic phase diagram has been studied using ultrasonic techniques.<sup>9</sup>

Of particular interest are the properties that relate to the existence of a sizable gap in the antiferromagnetic magnon spectrum at  $\vec{k} = 0$ . For  $\text{MnF}_2$  this corresponds to a temperature  $T_{\text{AE}} = 12.5^\circ\text{K}$  at zero field. Perhaps the most dramatic consequence of the gap's presence is manifest in the temperature dependence of the nuclear spin-

lattice relaxation (NSLR) rate  $1/T_1$  of the  $^{19}\text{F}$  NMR at zero field.<sup>10</sup> There a variation of six orders of magnitude in  $^{19}(1/T_1)$  was found in the temperature range  $3.2\text{--}26^\circ\text{K}$ . It was this sensitivity which provided the initial motivation to use the nuclear relaxation as a tool for a detailed investigation of the field dependence of the excitation spectra, particularly close to the "spin-flop" transition  $H_{\text{SF}}$  ( $H_{\text{SF}} \approx 93 \text{ kOe}$ ), where the energy of one of the two magnon branches at  $\vec{k} = 0$  vanishes as  $H_0$  approaches  $H_{\text{SF}}$ .

We report here on a combined experimental and theoretical study of the field dependence of both the  $^{19}\text{F}$  and  $^{55}\text{Mn}$  NSLR at  $4.2^\circ\text{K}$ , where  $T \ll T_N$  ( $T_N = 67.3^\circ\text{K}$ ). The results obtained provide a quantitative confirmation of the predictions of spin-wave theory at all fields *except* in the immediate vicinity of  $H_{\text{SF}}$  where there is evidence for anomalous "critically like" behavior, particularly for the  $^{55}\text{Mn}$  NMR where a  $(H_{\text{SF}} - H_0)^{-3/2}$  divergence in  $1/T_1$  is found.

In Sec. II, the electronic and nuclear magnetic interactions in  $\text{MnF}_2$  are used to construct appropriate exchange and hyperfine Hamiltonians. Section III describes the experimental apparatus and procedure and Sec. IV the results of NSLR measurements as a function of field, for both  $^{19}\text{F}$  nuclei and  $^{55}\text{Mn}$  nuclei in pure  $\text{MnF}_2$ . In Sec. V, after a brief review of the necessary spin wave theory, a theoretical interpretation is given of the observed  $^{19}\text{F}$  NSLR in terms of the Raman scattering of spin waves and the  $^{55}\text{Mn}$  NSLR as results from three-magnon exchange-enhanced scattering. The anomalous behavior of the NSLR in the vicinity

of  $H_{SF}$  is shown to be consistent with a direct process involving damped magnons. An effective-field theory is developed that predicts a  $(H_{SF} - H_0)^{-1}$  dependence to  $\chi_{\perp}$  and the rf-field enhancements, with  $\vec{H}_0 \parallel \hat{c}$ . Appendix A contains a comparison of the small- $\vec{k}$  and spherical-model calculation of the density of states with one that is relatively exact for  $MnF_2$ . The importance of this to the temperature dependence of NSLR rates is demonstrated. A "thermally weighted density of states" procedure is used to show which regions of the Brillouin zone dominate the NSLR for various temperature and fields. Finally in Appendix B we report on related experimental and theoretical work on the NSLR rates of  $^{19}F$  nuclei adjacent to nonmagnetic impurities in  $MnF_2:Zn$  and show this to be consistent with, and lend support to, the interpretation given for the pure-crystal experiments.

## II. ELECTRONIC AND NUCLEAR MAGNETIC PROPERTIES OF $MnF_2$

$MnF_2$  crystallizes in the body-centered tetragonal rutile structure with  $c/a=0.68$ .  $Mn^{2+}$  ions are located at  $(0, 0, 0)$  and  $(\frac{1}{2}, \frac{1}{2}, \frac{1}{2})$  and the  $F^-$  ions at  $\pm(u, u, 0)$ ,  $(\frac{1}{2} \pm u, \frac{1}{2} \mp u, \frac{1}{2})$  in the unit cell, and  $u=0.31a$ . Below the Néel temperature ( $T_N = 67.3^\circ K$ ) and for magnetic fields applied parallel to the  $c$  axis which are less than the "spin-flop" field, the  $Mn^{2+}$  electronic spins order as an easy-axis two-sublattice antiferromagnet (i.e., the moments at the body-center and corner-site positions are oppositely directed along the crystal-line  $c$  axis, as shown in Fig. 1). The size of the chemical and magnetic unit cells are identical.

### A. Electronic interactions

The exchange, anisotropy, and Zeeman interactions for  $MnF_2$  may be represented by the Hamiltonian

$$\mathcal{H}_e = 2J_1 \sum_{nn} \vec{S}_i \cdot \vec{S}_{i'} + 2J_2 \sum_{nnn} \vec{S}_i \cdot \vec{S}_j - \frac{K}{2} \left[ \sum_i (\vec{S}_i^z)^2 + \sum_j (\vec{S}_j^z)^2 \right] - g\mu_B H_0 \left( \sum_i \vec{S}_i^z + \sum_j \vec{S}_j^z \right), \quad (2.1)$$

where the isotropic exchange interaction extends to the  $z_1=2$  nearest neighbors (nn) and  $z_2=8$  next nearest neighbors (nnn). The exchange between third nn is negligible. It is an approximation to represent the anisotropy in single-ion form, as above, since in fact, it is mainly dipolar in character. However,  $K$  is a phenomenological constant accurately determined from perpendicular susceptibility,<sup>3</sup> antiferromagnetic resonance,<sup>7</sup> and neutron-scattering<sup>2</sup> experiments and the wave-vector ( $\vec{k}$ ) dependence of single-ion and dipolar anisotropy differ little at those relatively small values of  $\vec{k}$  which dominate the thermodynamic properties at  $T \ll T_M$ . Thus the approximation of replacing the dipolar anisotropy by the simpler single-ion form is most satisfactory for our purposes. Values of the exchange and anisotropy parameters are given in Table I. To remove any ambiguity as to the origins of the values chosen, the equations from which they are derived, both with and without zero-point spin-wave corrections, are given in the caption for Table I. It is sometimes useful to represent  $J$  and  $K$  as effective fields, to wit,  $H_E = 2J_2 Z_2 S / g\mu_B$ ,  $H_A = KS / g\mu_B$ . Values of all these parameters as well as the field  $H_{SF}$  where spin flop occurs are also contained in the table. The fact that  $|Z_2 J_2| \gg |Z_1 J_1|$  and  $J_2 > 0$  combined with  $K > 0$  results in  $MnF_2$  being an almost ideal two-sublattice easy-axis antiferromagnet.

Regarding the spin-flop transition some subtlety exists as to precisely the field at which it takes place. Because of its importance as to the maxi-

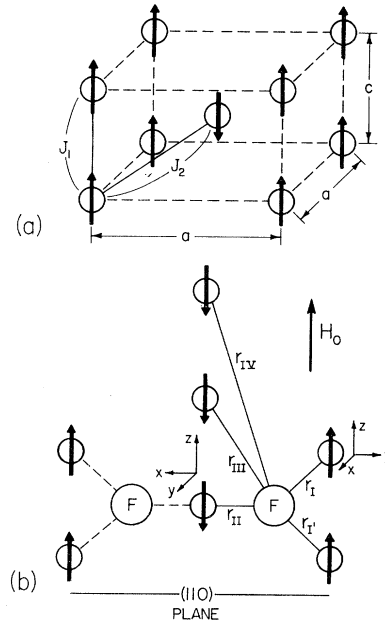


FIG. 1. Magnetic structure of antiferromagnetic  $MnF_2$ . (a) The direction of  $Mn^{2+}$  spin ordering is shown together with an illustration of the exchange couplings  $J_1$  and  $J_2$ . (b) The local  $^{19}F$  nuclear site symmetry is shown. The small coordinate axes define the principle axes of the  $^{19}F$  hyperfine tensors with respect to the type-I and -II  $Mn^{2+}$  spins. Type-III and -IV  $Mn^{2+}$  sites are exhibited as examples of electronic sites which can give significant contributions to  $^{19}(1/T_1)$  via the  $Mn^{2+}-^{19}F$  dipole interaction.

mum  $H_0$  at which NMR can be studied in the anti-ferromagnetic state we briefly give some details. Zero-point effects are omitted from the following considerations. With  $H_0$  exactly parallel to the  $c$  axis it is observed<sup>11</sup> that macroscopic samples develop a domain structure of alternating anti-ferromagnetic and spin-flop character at a field  $H_D$  defined by

$$H_D^2 = 2H_E H_A - H_A^2 - \frac{8}{3}\pi M_s H_A, \quad (2.2)$$

where  $M_s$  is the sublattice magnetization and the last term is the Lorentz field correction. This transition to the mixed state is almost 1 kOe lower than the so-called spin-flop field  $H_{\text{SF}}$  defined by

$$H_{\text{SF}}^2 = 2H_E H_A + H_A^2 + (N_{\perp} - \frac{4}{3}\pi) 2M_s H_A. \quad (2.3)$$

Here  $N_{\perp}$  is the demagnetizing factor perpendicular to the  $c$ -axis direction and we have assumed that  $T \ll T_N$  so that  $\chi_{\parallel}$  is negligible. Both the theoretical predictions for the NSLR and the divergence of  $\chi_{\perp}$  are developed with respect to  $H_{\text{SF}}$  although, in fact, the transition to the mixed state at  $H_D$  precludes the possibility of making comparisons between experiment and theory beyond  $H_D$ .

#### B. $^{19}\text{F}$ and $^{55}\text{Mn}$ hyperfine interactions

In the conceptually simplest case of an  $I = \frac{1}{2}$  nucleus interacting *only* with the spin moment of its own atomic electrons the hfs interaction in a solid has the form

$$\mathcal{H}_n = \vec{I} \cdot \vec{A} \cdot \vec{S} = A_{zz} I_z S_z + A_{xx} I_x S_x + A_{yy} I_y S_y. \quad (2.4)$$

For antiferromagnetically ordered systems, with the directions of quantization for the electrons and nuclear moments collinear along the  $z$  direction, the resonance frequencies in a field  $\vec{H}_0 \parallel \vec{z}$  are

$$h\nu_{\pm} = A_{zz} \langle S_z \rangle_{T, H_0} \pm \gamma H_0, \quad (2.5)$$

where  $\langle S_z \rangle_{T, H_0}$  is the thermal average of the spin magnetization at  $T$  and  $H_0$  and  $\gamma$  is the nuclear gyromagnetic ratio. The transverse components of  $\mathcal{H}_n$ —the terms involving  $I_x$  and  $I_y$ —would be responsible for inducing transitions between nuclear states  $M_I = \pm \frac{1}{2}$  and are therefore instrumental in the NSLR process.

The generalization of the above remarks to the specific cases of the  $^{19}\text{F}$  and  $^{55}\text{Mn}$  NMR in  $\text{MnF}_2$  have been given<sup>12,13</sup> and we abstract only those details which are necessary to understanding the resonance frequencies and the relaxation processes.

#### I. $^{19}\text{F}$ hfs

The hfs Hamiltonian for the  $^{19}\text{F}$  ( $I = \frac{1}{2}$ ) NMR in a dc field  $\vec{H}_0 \parallel \hat{z}$  may be expressed as follows:

$$\begin{aligned} {}^{19}\mathcal{H} = & \left( \sum_{i=1}^3 A_{zz}^i + \sum_{i=4}^N D_{zz}^i \right) I_z S_z \pm {}^{19}\gamma H_0 I_z \\ & + \left( \sum_{i=1}^3 A_{yz}^i + \sum_{i=4}^N D_{yz}^i \right) I_y S_z \\ & + \sum_{i=1}^3 (A_{xx}^i I_x S_x^i + A_{yy}^i I_y S_y^i). \end{aligned} \quad (2.6)$$

Reference should be made to Fig. 1 where the local  $\text{Mn}^{2+}$  coordination about a  $\text{F}^-$  is shown. The largest part of the hfs arises from the transferred hyperfine interaction with the three nn to a given  $\text{F}^-$  ion; hence the partitioning of these seen above. The term  $A_{yz}^i$  appears because the hfs tensor is nondiagonal in the chosen set of axes.

The various components of the  $D_{ik}^i$  represent the dipolar interactions with a spin  $\vec{S}^i$ , at position  $\vec{r}^i$  with respect to the  $^{19}\text{F}$  nucleus, *other* than the three nearest  $\text{Mn}^{2+}$  neighbors. All terms  $D_{ik}^i$ , with  $l \neq y, k \neq z$ , have been deliberately omitted since they neither contribute to determining the resonance frequency nor significantly affect the relaxation. The  $(\pm)$  in the Zeeman contribution shows that  $H_0$  either adds or subtracts from the local field produced by the hfs interaction and corresponds to there being two magnetically inequivalent  $\text{F}^-$  sites with  $\vec{H}_0 \parallel \hat{z}$ . The generalization of Eq. (2.5) results in the following expression for the two  $^{19}\text{F}$  NMR frequencies:

$$h\nu_{\dagger\ddagger} = \left( (2A_{zz}^I - A_{zz}^{II}) + \sum_{i=4}^N D_{zz}^i \right) \langle S_z \rangle_{T, H_0} \pm {}^{19}\gamma H_0 \quad (2.7)$$

where the  $\dagger(\ddagger)$  corresponds to the branch which initially increases (decreases) with  $H_0$ . Numerical

TABLE I. Values of the exchange and anisotropy parameters appropriate to  $\text{MnF}_2$  and the Hamiltonian given in Eq. (2.1).  $J_2$  and  $K$  are derived from experimental measurements of the antiferromagnetic-resonance frequency (Ref. 7) and  $\chi_{\perp}$  (Ref. 3) extrapolated to  $T = 0$  °K, using the zero-point corrected relations (Ref. 1) for those quantities:  $(g\mu_B H_{\text{SF}})^2 = (h\nu_0)^2 = K S^2 (4ZJ + K) \times \{1.0292\}^2$  and  $\chi_{\perp} = N g^2 \mu_B^2 (4ZJ + K)^{-1} \{0.9617\}$ .  $J_1$  was determined from neutron-scattering studies (Ref. 2). From these relations one derives the quantities  $H_A$  and  $H_E$  shown as (a). The classical values shown as (b) are obtained by neglecting the zero-point corrections contained in the curly brackets. (See complete discussion in Ref. 1.) The values shown in the table differ slightly from others used in the literature because of errors previously made in applying zero-point corrections.

|    | $J_1$ | $J_2$ | $K$   | $H_E$   | $H_A$ | $H_{\text{SF}}$ |
|----|-------|-------|-------|---------|-------|-----------------|
| °K | 0.32  | -1.78 | 0.415 | (a) 528 | 7.73  | 93.3            |
|    |       |       |       | (b) 550 | 7.87  | 93.3            |

values for the  $A_{iK}^i$  that are important to the present studies are given in Table II and in Fig. 2 a plot of Eq. (2.7) is shown.

## 2. $^{55}\text{Mn}$ hfs

The hfs Hamiltonian for the  $^{55}\text{Mn}$  ( $I = \frac{5}{2}$ ) NMR in a dc field  $\vec{H}_0 \parallel \hat{z}$  may be expressed as follows<sup>13</sup>:

$${}^{55}\mathcal{H} = \left[ \left( {}^{55}A_{zz} S_z + \sum_{i \neq 0}^N D_{zz}^i S_z^i \right) \pm {}^{55}\gamma H_0 \right] I_z + {}^{55}A_{xx} I_x S_x + {}^{55}A_{yy} I_y S_y + \mathcal{H}_Q, \quad (2.8)$$

where  $\mathcal{H}_Q$  is the quadrupolar part of the Hamiltonian. All of the components  ${}^{55}A_{jj}$  of the hyperfine tensor are large and approximately equal to each other.<sup>14</sup> Again the  $D_{zz}^i$  are the dipolar contributions of a spin  $\vec{S}^i$  at position  $\vec{r}^i$  with respect to the  $^{55}\text{Mn}$  nucleus. Note that we have not included  $D_{lk}^i$  dipolar terms for which  $l \neq z, k \neq z$ . The reason for this is that  $|D_{lk}^i / {}^{55}A| \approx 10^{-2}$  and while a 1% contribution is easily measured in the NMR frequency, it has an insignificant effect on the relaxation processes.

The generalization of Eq. (2.8) results in the following expressions for the two  $^{55}\text{Mn}$  NMR frequencies corresponding to the transition

$$(m_I = +\frac{1}{2} \rightarrow -\frac{1}{2}):$$

$$h\nu_{\uparrow\downarrow}(\frac{1}{2} \leftrightarrow -\frac{1}{2}) = \left( {}^{55}A_{zz} + \sum_{i \neq 0}^N D_{zz}^i \right) \langle S_z \rangle_{T, H_0} \pm {}^{55}\gamma H_0 \quad (2.9)$$

where the  $\uparrow(\downarrow)$  corresponds to the branch which decreases (increases) with  $H_0$ . Numerical values for the  $^{55}\text{Mn}$  parameters are given in Table II, and in Fig. 2 a plot of Eq. (2.9) is shown. [Since we

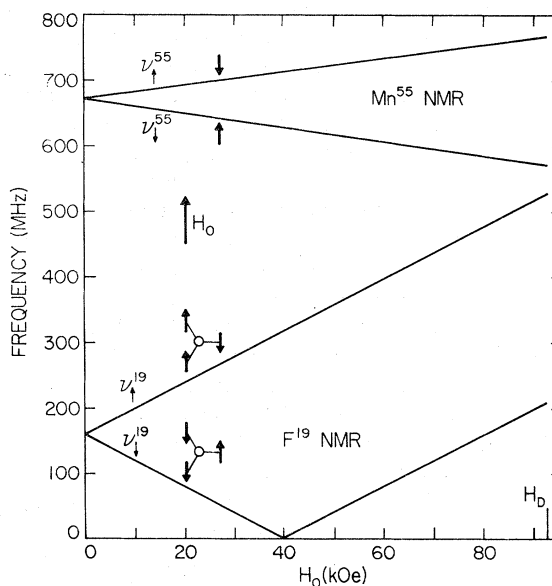


FIG. 2. Predicted (and observed) frequencies of the  $^{19}\text{F}$  and  $^{55}\text{Mn}$  NMR in  $\text{MnF}_2$  at 4.2 °K as a function of external field  $\vec{H}_0 \parallel \hat{z}$ . The direction of the  $\text{Mn}^{2+}$  spin moments associated with each of the resonances relative to  $H_0$  is also shown as is the notation used for the "up-going" and "down-going"  $^{19}\text{F}$  and  $^{55}\text{Mn}$  NMR branches.

are not presently interested in the quadrupolar effects we will henceforth drop the notation  $(\frac{1}{2} \leftrightarrow -\frac{1}{2})$  in referring to this central resonance of the quadrupolar split group of five resonances.] The reversal of the signs notation in going from the  $^{19}\text{F}$  to  $^{55}\text{Mn}$  NMR is a direct consequence of the negative sign of  ${}^{55}A$ ;  ${}^{19}A$ ,  ${}^{19}\gamma$  and  ${}^{55}\gamma$  are all positive.

TABLE II. The  $^{19}\text{F}$  and  $^{55}\text{Mn}$  hfs components in  $\text{MnF}_2$ . The symmetry axes of the  $^{19}\text{F}$  hfs tensor are shown in Fig. 1. The necessary components of the dipole tensor for the interaction of a given  $^{19}\text{F}$  nucleus with the  $i$ th  $\text{Mn}^{2+}$  spin at  $\vec{r}_i$  are also given. Reference to Fig. 1 should be made for the identification of a particular  $\text{Mn}^{2+}$  spin. The vector  $\vec{r}_i$  has its origin at the type-II  $\text{Mn}^{2+}$  site, and "sublattice" is defined with respect to the type I sites.

|                            |            | Hyperfine components                           |               |               |  |  |
|----------------------------|------------|--|---------------|---------------|--|--|
| (cm <sup>-1</sup> )        |            | $A_{xx}^{19}$                                  | $A_{yy}^{19}$ | $A_{zz}^{19}$ | $A_{yz}^{19}$                                  | $A^{55}$   |
| Type I                     | $10^{-4}$  | 11.81  | 15.57         | 17.83         | 4.4  | 92.3   |
| Type II                    | $10^{-4}$  | 23.34  | 13.44         | 12.90         | 0.0  |  |
|                            |            | Off-diagonal $^{19}\text{F}$ dipole components |               |               |  |  |
| $D_{yz}^i$                 | III, III'  | IV, IV'  | V, V'         | V'', V'''     | VI, VI'  | VI'', VI'''                                      |
| sublattice                 | other      | other  | other         | same          | same   | same   |
| $\vec{r}_i$                | (0, 0 ± 1) | (0, 0 ± 2)                                     | (1, 0 ± 1)    | (0, -1 ± 1)   | ( $\frac{1}{2}, \frac{1}{2} \pm \frac{1}{2}$ ) | ( $-\frac{1}{2}, -\frac{1}{2} \pm \frac{1}{2}$ ) |
| value                      |            |  |               |               |  |  |
| $10^{-4}$ cm <sup>-1</sup> | 0.550      | 0.063  | 0.132         |               | 0.152  |  |

Because the  $^{19}\text{F}$  nuclear hyperfine-coupling constants are positive, the hyperfine field at any  $^{19}\text{F}$  site points *parallel* to the direction of the electronic moments at the two neighboring type-I electronic sites. Therefore the  $^{19}\text{F}$  nuclear resonance which initially increases ("upgoing") in frequency with increasing magnetic field is associated with two type-I  $\text{Mn}^{2+}$  moments which are oriented parallel and one type-II  $\text{Mn}^{2+}$  moment which is oriented antiparallel to the external field. By way of contrast, because the  $^{55}\text{Mn}$  hyperfine-coupling constants are negative, the "upgoing"  $^{55}\text{Mn}$  nuclear-resonance branch is associated with an electronic moment which is oriented antiparallel with the external field. The association of the "downgoing" nuclear-resonance branches with magnetic-moment orientations is obtained from the "upgoing" NMR branches by simply inverting all of the electronic moments. (We belabor this point because it is essential in the interpretation of the nuclear-relaxation data, as the magnitude of the fluctuations associated with electronic moments ordered parallel to the external field are different in magnitude from those of the antiparallel moments.)

### III. EXPERIMENTAL PROCEDURE

Nuclear-spin-lattice-relaxation measurements have been performed as a function of magnetic field  $H_0$  from  $H_0=0$  up to fields close to  $H_D$ . At 4.2 °K, and for this range of  $H_0$  applied parallel to the crystalline  $c$  axis, the  $^{55}\text{Mn}$  NMR occurs in the range 570–770 MHz and the  $^{19}\text{F}$  NMR lies between zero and 530 MHz.

Most of the  $^{19}\text{F}$  NMR data were taken using high-power incoherent spin-echo techniques. The spectrometer itself is similar to one described before<sup>15</sup> except that a high-quality field-effect transistor (FET) input communications receiver was used, and 90° hybrid couplers and a limiter were used for receiver isolation and protection. In addition, tuning stubs and adjustable lines were used as a convenient means of impedance matching over the large range of  $^{19}\text{F}$  NMR frequencies investigated.

All of the NSLR measurements were made using saturation-recovery techniques. The relaxation was always well fit by an exponential relaxation rate with a characteristic relaxation rate  $T_1$ ,

$$M(t) = M(\infty)(1 - e^{-t/T_1}).$$

In the spin-echo measurements, the nuclear magnetization was saturated by a "comb" of rf pulses. At a time  $t$  later the nuclear magnetization  $M(t)$  was measured by observing the amplitude of the echo following a two-pulse sequence. Repetition of these measurements for various values

of  $t$  and  $t \gg T_1$  (i.e.,  $t = \infty$ ) gives a value for  $T_1$ . At frequencies higher than about 350 MHz less than half of the rf power from the 90° hybrid was coupled properly into the sample coil due to losses or leakage in the tuning stubs network. This problem led in some measurements to inadequate nuclear saturation and poorer data. Hence data were retaken using the cw technique, described below, which was generally found to give more repeatable and therefore more reliable results at the higher frequencies. Each data point that is shown for the  $^{19}\text{F}$  relaxation at a given  $H_0$  involves an average over several sequential measurements. The quoted error of  $\pm 20\%$  is a liberal estimate of the maximum scatter in the individual measurements.

All of the measurements associated with the  $^{55}\text{Mn}$  NMR were made using cw NMR techniques. The cw spectrometer is of the rf bridge type, using rf phase-sensitive (homodyne) detection and low-noise broadband rf amplification. 180° hybrid junctions are used both for the bridge element and for isolation between reference and signal arms. A double-balanced mixer serves as the phase-sensitive detector. All components are broadband (10–1000 MHz) and matched to 50- $\Omega$  impedance.

To observe the weak  $^{55}\text{Mn}$  NMR at low fields where the enhancement is low, it was necessary to use a high- $Q$  (700) resonator with both frequency and coupling adjustment capacitors in the Dewar, close to the sample, remotely tunable from above. With this arrangement both large  $h_1$  for saturation and good sensitivity were available. Closer to spin flop ( $H_0 > 70$  kOe) the enhancements become so large that the signal seriously loaded the resonant circuit. Here it was possible to use a sample coil with inductance  $L$  and distributed capacitance  $C$  adjusted to give a transmission-line response with characteristic impedance  $Z_0 = (L/C)^{1/2}$  equal to the rf system impedance. When this coil is terminated in  $Z_0$ , good bridge balance is possible from 0 to 1 GHz. The time delay  $\tau = (L/C)^{1/2}$  determines the maximum operating frequency. Although the effective  $Q$  of this system is of the order of 1 it gives adequate signals in the region where large enhancements are observed.

The cw  $T_1$  measurements were made by saturating the nuclear magnetization at maximum rf power level, then monitoring continuously its recovery with low rf power. When  $T_1$  was long enough ( $T_1 > 1$  sec) the switching from high to low rf power was done manually. Field modulation and lock-in detection was used, with derivative signals displayed on a chart recorder. For  $T_1$ 's shorter than 1 sec, the switching was done with a PIN diode modulator driven by a square wave,

and the dc mixer output was displayed on an oscilloscope. Signal averaging was used to improve signal to noise ratios.

In the frequency-pulling region (see Sec. IV), the NMR lines shifted by more than their width upon saturation. Extremely nonexponential recoveries resulted from monitoring the peak of the lines. Reasonable results were obtained by monitoring the most linear region of the side of the line, which converts the shift to an amplitude change. Since only one time constant  $T_1$  is involved, this procedure gives correct values for  $T_1$ .

For two reasons, it was necessary to align the  $c$  axis of the sample very precisely parallel with the applied field. First, for misalignments of the order of  $\frac{1}{2}^\circ$  or more the electronic spins monotonically tip from the antiferromagnetic to the spin-flop orientation and the sample does not exhibit the sharp transition near  $H_D$  which is of interest here. Second, misalignment of the electronic spins with the  $c$  axis below spin-flop allows an otherwise forbidden  $^{19}\text{F}$  relaxation<sup>10</sup> process. Data analysis for the  $^{19}\text{F}$  NSLR is more straightforward if this extra source of relaxation is made negligible by maintaining good sample alignment. Sample alignment was obtained with the sample in position in the magnet and while observing the  $^{19}\text{F}$  NMR within a few kilogauss of  $H_D$ . Because of the highly anisotropic  $^{19}\text{F}$  hyperfine field, and because the direction of electronic spin alignment is a very strong function of sample misalignment for  $H_0$  near  $H_D$ , it was possible to align the crystalline  $c$  axis parallel to  $H_0$ , by adjusting the sample alignment until the downgoing  $^{19}\text{F}$  branch occurred at the lowest possible frequency for a fixed field, or at the highest possible field for a fixed frequency. Using this technique it was possible to align the sample  $c$  axis parallel to  $H_0$  to within about  $0.1^\circ$  or better.

NSLR measurements at fields less than 25 kOe were made at  $4.2^\circ\text{K}$  in a standard research Dewar mounted in an iron electromagnet. All of the higher-field measurements were made in a superconducting solenoid. The Dewar associated with the solenoid was fitted with a thin-wall stainless-steel tube which provided access to the magnet core while excluding the liquid helium. For measurements at  $4.2^\circ\text{K}$  an atmosphere of helium gas in the tube provided excellent thermal contact with the liquid-helium bath. It was possible to obtain higher sample temperatures by putting the sample in thermal contact with a resistance heater while reducing the thermal conductance to the helium bath by evacuating the access tube. Temperature control was obtained by using a magnetic-field-independent capacitance thermometer in an ac bridge circuit and using voltages from

the bridge imbalance to control the power delivered to the heater. Although temperature control was adequate ( $\pm 0.1^\circ\text{K}$ ), the actual sample temperature was somewhat lower than that at the thermometer. Temperatures higher than  $4.2^\circ\text{K}$  were thus estimated by extrapolating the theoretical  $H_0$  dependence of  $^{19}(1/T_1)$  to  $H_0 = 0$  and comparing with measurements<sup>10</sup> there. In the superconducting solenoid coarse magnetic-field measurement was obtained from a copper magnetoresistance coil in the body of the magnet. Accurate field measurement was made using the  $^{19}\text{F}$  NMR in Teflon in a small untuned sample coil similar to that used in the cw NMR experiments as described above. In the  $^{19}\text{F}$  experiments the NMR magnetometer was mounted radially outwards in the solenoid 8 mm away from the  $\text{MnF}_2$  sample which corresponded to a field higher than that at the sample by 0.04% (36 Oe at 90 kOe). It was necessary to take this correction into account to obtain the field at the sample itself.

## IV. EXPERIMENTAL RESULTS

### A. NSLR

The NSLR rate  $1/T_1$  was measured as a function of field from  $H_0 = 0$  to  $H_D$  at  $4.2^\circ\text{K}$  for both branches of the  $^{19}\text{F}$  and  $^{55}\text{Mn}$  NMR. These data are shown in Figs. 3 and 4 and are seen to exhibit certain qualitatively similar features. The relaxation rates of the two NMR branches for both nuclei

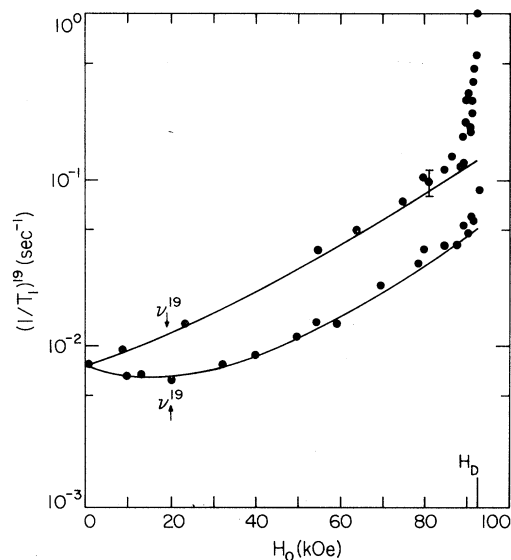


FIG. 3. Nuclear spin-lattice relaxation rate for the  $^{19}\text{F}$  NMR in  $\text{MnF}_2$  at  $4.2^\circ\text{K}$  as a function of  $H_0 \parallel \hat{c}$ . The dots are the experimental observations and the solid lines are the predictions of the detailed two-magnon theory.

showed a marked increase as  $H_0$  was increased significantly above zero. Again for both the  $^{55}\text{Mn}$  and  $^{19}\text{F}$  nuclei, the branch with the faster of the two relaxation rates corresponds to those nuclei associated with the magnetic sublattice whose electronic moments point *opposite* to the direction of the magnetic field.

As  $H_0$  approaches  $H_D$ , quite striking behavior is observed in the relaxation rates. For both  $^{55}\text{Mn}$  NMR branches a very sharp increase in the relaxation rates is observed with  $1/T_1$  rising by more than an order of magnitude within an interval of 3 kOe of  $H_D$ . Throughout the high-field region the ratio of the relaxation rates of the two branches remains about 2.5. The peak in  $1/T_1$  in the  $^{19}\text{F}$  data near  $H_D$  shows significantly different behavior. Whereas the relaxation rate on the downgoing  $^{19}\text{F}$  branch increases by almost an order of magnitude within an interval of about 3 kOe near  $H_D$ ,  $1/T_1$  on the upgoing  $^{19}\text{F}$  branch shows little or no such increase. This disparity in the relative mag-

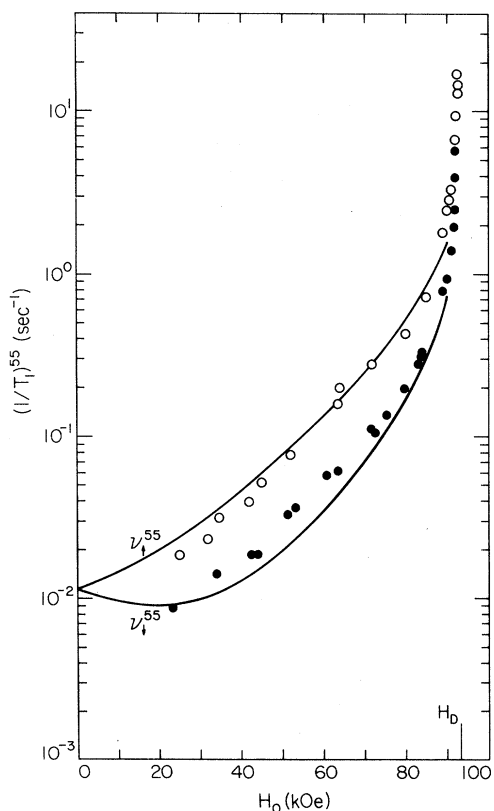


FIG. 4. Nuclear spin-lattice relaxation rates for the  $^{55}\text{Mn}$  NMR in  $\text{MnF}_2$  at 4.2 °K as a function of  $H_0 \parallel \hat{c}$ . The circles represent the experimental observations; the solid lines are the predictions of the three-magnon theory of Freyne and Pincus normalized to agree with the experimental results in the region 40–80 kOe.

nitudes of the relaxation close to  $H_D$  on the two  $^{19}\text{F}$  resonance branches will be discussed in detail in Sec. V.

As will be shown, the sharp increase in the relaxation rate near  $H_D$  for both  $^{19}\text{F}$  and  $^{55}\text{Mn}$  nuclei is not explained by spin-wave-theory calculations for two- and three-magnon relaxation processes as discussed in Sec. V, and hence the behaviors in this region are referred to as “anomalous” in both cases.

Additional experiments were performed on the anomalous peak in the  $^{19}\text{F}$  relaxation on the downgoing branch in order to elucidate its qualitative behavior. Measurements were made at two higher temperatures  $T = 5.8$  and  $7.8$  °K with the purpose of obtaining information on the temperature dependence of  $1/T_1$  near spin-flop relative to the relaxation rate at lower fields. These data are shown in Fig. 5. One feature of the data is immediately apparent from the figure; namely, the relative *decrease* in the magnitude of the anomalous contribution as the temperature is *increased*. Since the relaxation at higher temperatures becomes increasingly dominated by excitations with larger  $\vec{k}$  (see Appendix A) it is clear that the anomalous behavior observed must be associated with relatively small- $\vec{k}$  excitations of the spin system.

#### B. $^{55}\text{Mn}$ NMR

At fields below  $\sim 50$  kOe a symmetrical spectrum of five quadrupole lines was observed, with widths and relative amplitudes in agreement with the

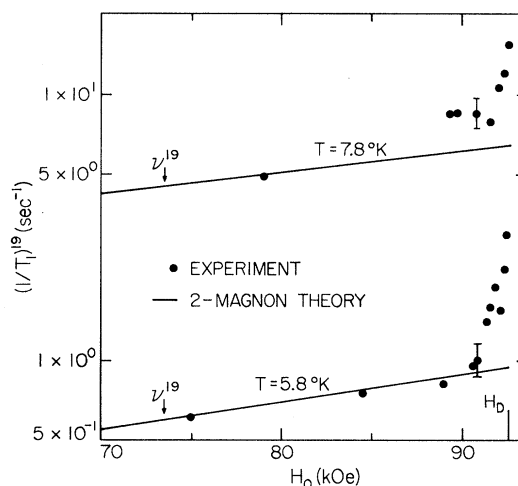


FIG. 5. Nuclear spin-lattice relaxation rate for the  $^{19}\text{F}$  NMR ( $^{19}\text{F}_1$  branch) in  $\text{MnF}_2$  at 5.8 and 7.8 °K in the range of external fields 70–92 kOe. The dots are the experimental observations and the solid curves are the detailed predictions of the two-magnon theory.

Suhl-Nakamura<sup>16,17</sup> theory and previous experiments.<sup>13</sup> At higher fields, a field scan gives an unsymmetrical quadrupole spectrum due to the field dependence of the enhancement across the spectrum. Close to  $H_D$ , the divergent susceptibility  $\chi_\perp$  detunes the NMR coil, while losses associated with  $\chi_\perp$  appear as a huge nonresonant derivative signal centered about  $H_D$ . When NMR is done in this region, the nonresonant signal overlaps the NMR, and tuning of the NMR system is quite awkward.

In addition a series of unexplained effects was observed, which we tentatively identify with the field dependence of the Suhl-Nakamura interaction. (i) Above 60 kOe the center line of the quadrupole spectrum broadens and disappears from the derivative spectrum. (ii) Above 85 kOe the lower-frequency quadrupole component grows in amplitude relative to the others until it entirely dominates the spectrum. (iii) For  $H_D - H_0 < 1$  kOe, frequency-pulling effects<sup>18</sup> are observed upon saturation of the NMR. The above effects are more pronounced, and occur at lower fields, on the  $^{55}\nu_+$  NMR branch. The fields quoted above apply to the  $^{55}\nu_+$  branch.

### C. Enhancements

In both the  $^{19}\text{F}$  and  $^{55}\text{Mn}$  NMR experiments an enhancement of the applied rf field was observed which increased with increasing field. A rough measure of the  $^{19}\text{F}$  enhancements was obtained by observing the requisite widths of a pair of pulses selected so as to optimize the nuclear spin-echo signal. In the  $^{55}\text{Mn}$  case the enhancements were estimated on the basis of the relative size and saturation of the NMR signal, assuming the enhancement to be virtually zero when  $H_0 = 0$ . Defining the enhancement  $\eta$ , such that  $H_{\text{eff}} = H_{\text{rf}} \times (1 + \eta)$ , we find the values that are shown in Table III. These are compared with the predictions obtained from the theory developed in Sec. VC.

## V. THEORY AND DISCUSSION

### A. Spin-wave theory

The spin-wave theory appropriate to describing the thermodynamic properties of antiferromagnets

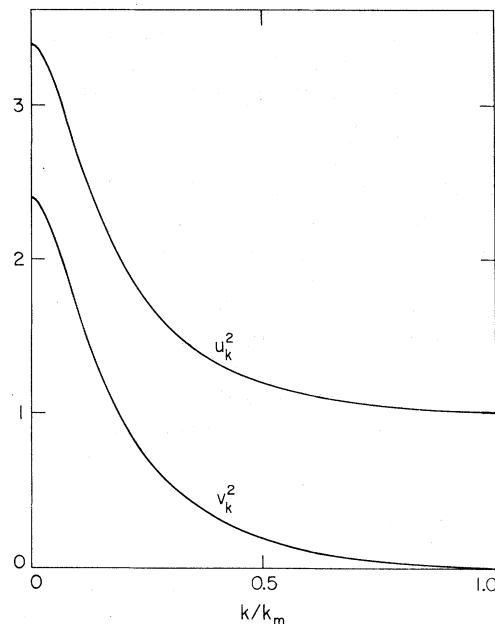


FIG. 6. Variations of the transformation coefficients  $u_{\vec{k}}^2$  and  $v_{\vec{k}}^2$  in  $\text{MnF}_2$  as a function of  $\vec{k}$  in the [100] direction [after R. Loudon, Adv. Phys. **17**, 243 (1968)]. Since  $u_{\vec{k}}^2 = \frac{1}{2}[2J_2 z S(1 + \xi_0) + \hbar\omega_{\vec{k}}]/\hbar\omega_{\vec{k}}$  and  $v_{\vec{k}}^2 = \frac{1}{2}[2J_2 z S(1 + \xi_0) - \hbar\omega_{\vec{k}}]/\hbar\omega_{\vec{k}}$ , one finds for the small- $k$  region,  $u_{\vec{k}}^2 \approx u_0^2 = \frac{1}{2}[(H_B/2H_A)^{1/2} + 1]$  and  $v_{\vec{k}}^2 \approx v_0^2 = \frac{1}{2}[(H_B/2H_A)^{1/2} - 1]$ .

is well known.<sup>1,19</sup> We briefly outline only those aspects of the theory that are essential to the discussion of the nuclear relaxation in  $\text{MnF}_2$ .

Starting with the Hamiltonian Eq. (2.1), spin-deviation operators are defined in the Holstein-Primakoff representation<sup>20</sup> as follows:

$$\begin{aligned} S_i^+ &= (2S - a_i^\dagger a_i)^{1/2} a_i, & S_j^+ &= b_j^\dagger (2S - b_j^\dagger b_j)^{1/2}, \\ S_i^- &= a_i^\dagger (2S - a_i^\dagger a_i)^{1/2}, & S_j^- &= (2S - b_j^\dagger b_j)^{1/2} b_j, \\ S_i^z &= (S - a_i^\dagger a_i), & S_j^z &= -S + b_j^\dagger b_j, \end{aligned} \quad (5.1)$$

where  $a_i^\dagger, b_j^\dagger$  ( $a_i, b_j$ ) create (destroy) spin deviations on specific sites on each of the two sublattices. Linear spin-wave theory is generated by expressing the Hamiltonian in terms of the Fourier-transformed spin-wave operators  $a_{\vec{k}}^\dagger, a_{\vec{k}}, b_{\vec{k}}^\dagger, b_{\vec{k}}$  where, for example,

$$a_{\vec{k}}^\dagger = \frac{1}{\sqrt{N}} \sum e^{i\vec{k} \cdot \vec{r}_i} a_i^\dagger, \quad b_{\vec{k}}^\dagger = \frac{1}{\sqrt{N}} \sum e^{-i\vec{k} \cdot \vec{r}_j} b_j^\dagger, \quad (5.2)$$

TABLE III. Approximate values of rf enhancements,  $\eta \equiv H_{\text{eff}}/H_{\text{rf}} - 1$ , as a function of applied field  $H_0$  for the  $^{19}\text{F}$  and  $^{55}\text{Mn}$  NMR in  $\text{MnF}_2$ . Values are obtained from Ref. 14.

| $H_0$ (kOe) | < 85  | 89-90       | $\leq 92.4$ | $H_0$ (kOe) | 50-60       | 87    | $\leq 92.4$ |                |            |
|-------------|-------|-------------|-------------|-------------|-------------|-------|-------------|----------------|------------|
| $^{19}\eta$ | Expt  | $\approx 0$ | $\approx 1$ | $\geq 5$    | $^{55}\eta$ | Expt  | 4-10        | $\approx 10^2$ | $\gg 10^3$ |
|             | Theor | 1           | 2           | 8.5         |             | Theor | 8           | 50             | 320        |

and retaining only linear and quadratic terms in these operators. This intermediate Hamiltonian is not diagonal but may be made so through the following Canonical transformation to new operators  $\alpha_{\vec{k}}^{\dagger}$ ,  $\alpha_{\vec{k}}^{\dagger}$ ,  $\beta_{\vec{k}}^{\dagger}$ , and  $\beta_{\vec{k}}^{\dagger}$

$$a_{\vec{k}}^{\dagger} = u_{\vec{k}}^{\dagger} \alpha_{\vec{k}}^{\dagger} - v_{\vec{k}}^{\dagger} \beta_{\vec{k}}^{\dagger}, \quad b_{\vec{k}}^{\dagger} = -v_{\vec{k}}^{\dagger} \alpha_{\vec{k}}^{\dagger} + u_{\vec{k}}^{\dagger} \beta_{\vec{k}}^{\dagger}. \quad (5.3)$$

The new Bose operators  $\alpha_{\vec{k}}^{\dagger}$ ,  $\beta_{\vec{k}}^{\dagger}$ , ( $\alpha_{\vec{k}}^{\dagger}$ ,  $\beta_{\vec{k}}^{\dagger}$ ) create (destroy) normal-mode spin-wave excitations in the antiferromagnetic system.

The transformation coefficients  $u_{\vec{k}}^{\dagger}$  and  $v_{\vec{k}}^{\dagger}$  are determined by imposing Bose commutation relations and by requiring that the off-diagonal components of the transformed Hamiltonian vanish. The transformation Eq. (5.3) is chosen so that  $u_{\vec{k}}^{\dagger}$  and  $v_{\vec{k}}^{\dagger}$  are both real and positive; the  $\vec{k}$  dependence of  $u_{\vec{k}}^{\dagger}$  and of  $v_{\vec{k}}^{\dagger}$  is shown in Fig. 6. The energies of the two resulting modes, neglecting zero-point effects, is

$$\hbar\omega_{\vec{k}}^{\dagger\dagger} = 2S_2J_2[(1 + \xi_{\vec{k}})^2 - \gamma_{\vec{k}}^2]^{1/2} \pm g\mu_B H_0, \quad (5.4)$$

where

$$\xi_{\vec{k}} = K/2Z_2J_2 - (2Z_1J_1/Z_2J_2) \sin^2 \frac{1}{2}ck_z, \quad (5.5)$$

$$\gamma_{\vec{k}} = \cos \frac{1}{2}ak_x \cos \frac{1}{2}ak_y \cos \frac{1}{2}ck_z, \quad (5.6)$$

and the  $\dagger(\ddagger)$  corresponds to modes of a given  $\vec{k}$  whose energy increases (decreases) with field.

The explicit relation between magnon operators and the individual spin operators may be obtained from Eqs. (5.1)–(5.3). For example, the operators that create excitations of a particular  $\vec{k}$  with either  $\Delta S_z = \pm 1$  for the whole spin system are

$$\alpha_{\vec{k}}^{\dagger} = (2SN)^{-1/2} \times \left( u_{\vec{k}}^{\dagger} \sum_i e^{-i\vec{k}\cdot\vec{r}_i} S_i^- + v_{\vec{k}}^{\dagger} \sum_j e^{i\vec{k}\cdot\vec{r}_j} S_j^- \right), \quad (5.7)$$

$$\beta_{\vec{k}}^{\dagger} = (2SN)^{-1/2} \times \left( u_{\vec{k}}^{\dagger} \sum_j e^{-i\vec{k}\cdot\vec{r}_j} S_j^+ + v_{\vec{k}}^{\dagger} \sum_i e^{i\vec{k}\cdot\vec{r}_i} S_i^+ \right).$$

From these equations and Fig. 6 it is clear that the creation of a magnon on either branch will involve almost equal excitations of spins on *both* sublattices near  $\vec{k}=0$ , while at  $\vec{k}=k_m$ , where

$$S_i^+ = \left( \frac{2S}{N} \right)^{1/2} \left[ \sum_{\vec{k}} e^{i\vec{k}\cdot\vec{r}_i} (u_{\vec{k}}^{\dagger} \alpha_{\vec{k}}^{\dagger} - v_{\vec{k}}^{\dagger} \beta_{\vec{k}}^{\dagger}) - (4SN)^{-1} \sum_{\vec{k}', \vec{k}'', \vec{k}'''} e^{i(\vec{k}' + \vec{k}'' - \vec{k}''')\cdot\vec{r}_i} (u_{\vec{k}'}^{\dagger} \alpha_{\vec{k}'}^{\dagger} - v_{\vec{k}'}^{\dagger} \beta_{\vec{k}'}^{\dagger}) (u_{\vec{k}''}^{\dagger} \alpha_{\vec{k}''}^{\dagger} - v_{\vec{k}''}^{\dagger} \beta_{\vec{k}''}^{\dagger}) (u_{\vec{k}'''}^{\dagger} \alpha_{\vec{k}'''}^{\dagger} - v_{\vec{k}'''}^{\dagger} \beta_{\vec{k}'''}^{\dagger}) + \dots \right], \quad (5.10a)$$

$$S_i^- = \left( \frac{2S}{N} \right)^{1/2} \left[ \sum_{\vec{k}} e^{i\vec{k}\cdot\vec{r}_i} (u_{\vec{k}}^{\dagger} \alpha_{\vec{k}}^{\dagger} - v_{\vec{k}}^{\dagger} \beta_{\vec{k}}^{\dagger}) - (4SN)^{-1} \sum_{\vec{k}', \vec{k}'', \vec{k}'''} e^{i(\vec{k} - \vec{k}' - \vec{k}'')\cdot\vec{r}_i} (u_{\vec{k}}^{\dagger} \alpha_{\vec{k}}^{\dagger} - v_{\vec{k}}^{\dagger} \beta_{\vec{k}}^{\dagger}) (u_{\vec{k}'}^{\dagger} \alpha_{\vec{k}'}^{\dagger} - v_{\vec{k}'}^{\dagger} \beta_{\vec{k}'}^{\dagger}) (u_{\vec{k}''}^{\dagger} \alpha_{\vec{k}''}^{\dagger} - v_{\vec{k}''}^{\dagger} \beta_{\vec{k}''}^{\dagger}) + \dots \right], \quad (5.10b)$$

$u_{\vec{k}}^{\dagger} \approx 1$  and  $v_{\vec{k}}^{\dagger} = 0$ , the zone-boundary magnons will propagate only on sublattice  $i(j)$  if  $\alpha_{\vec{k}}^{\dagger}$  ( $\beta_{\vec{k}}^{\dagger}$ ) is involved. Of course a continuous range of behavior exists between these simple extremes. We emphasize these points because the qualitative features of the field dependence of the  $^{19}\text{F}$  nuclear-relaxation rate may be immediately inferred from this subtle property of the  $\vec{k}$  dependence of  $u_{\vec{k}}^{\dagger}$  and  $v_{\vec{k}}^{\dagger}$ .

The operator which defines the number of magnons with energy  $\omega_{\vec{k}}^{\dagger}$  at temperature  $T$  is given in terms of the Bose factor as

$$\eta_{\vec{k}}^{\dagger} \equiv \langle \alpha_{\vec{k}}^{\dagger} \alpha_{\vec{k}}^{\dagger} \rangle = (e^{\hbar\omega_{\vec{k}}^{\dagger}/kT} - 1)^{-1}. \quad (5.8)$$

### B. Nuclear relaxation via magnon scattering

The NSLR process is the one by which an ensemble of nuclear spin moments reach thermal equilibrium with a "lattice" (in our case the magnon system) at temperature  $T$ . The standard procedure for calculating the rate  $(1/T_1)$  for this process is to regard the transverse part of  $\mathcal{H}_n$  as the perturbation Hamiltonian  $\mathcal{H}'_n$  and calculate the transition probability  $W$  according to the Golden Rule,

$$W = \frac{2\pi}{\hbar} \sum_f |\langle f | \mathcal{H}'_n | i \rangle|^2 \delta(E_i - E_f), \quad (5.9)$$

with

$$\frac{1}{T_1} = \frac{2W}{|\langle f | \mathcal{H}'_n | i \rangle|^2};$$

here  $\langle f |$  ( $|i\rangle$ ) and  $E_f$  ( $E_i$ ) represent final- (initial-) state wave functions and energies, respectively, of the combined nuclear- and electron-spin system. Energy conservation in the process is expressed in the  $\delta$  function  $\delta(E_f - E_i)$ .

The normal modes of the electronic system are magnons and hence the perturbation  $\mathcal{H}'_n$  must be expressed in terms of the magnon operators. Doing this naturally leads to a classification of the magnon-scattering processes that contribute to  $(1/T_1)$ . In the low-magnon-density limit the expansion of the square roots in the Holstein-Primakoff representation, Eq. (5.1), yields, for the  $i$  spin sublattice,

and  $S_i^z$  is directly given as

$$S_i^z = S - \frac{1}{N} \sum_{\vec{k}, \vec{k}'} e^{i(\vec{k} - \vec{k}') \cdot \vec{r}_i} (u_{\vec{k}} \alpha_{\vec{k}}^\dagger - v_{\vec{k}} \beta_{\vec{k}}^\dagger) (u_{\vec{k}'} \alpha_{\vec{k}'}^\dagger - v_{\vec{k}'} \beta_{\vec{k}'}^\dagger). \quad (5.10c)$$

Thus in the first-order linear theory in which one neglects magnon-magnon interactions there is a definite correspondence between the allowed magnon-nuclear spin-scattering processes and the single-spin operators that appear in  $\mathcal{H}'_n$ . If  $\mathcal{H}'_n$  contains only (a)  $S_i^+, S_i^-$ , then only *odd* numbers of magnons (1, 3, 5) may be scattered; (b)  $S_z$ , then only *two*-magnon scattering may take place.

Since the minimum spin-wave energy  $1/\hbar\omega_0$  is almost always such that  $\hbar\omega_0 \gg \hbar\omega_n$ , the direct or one-magnon process is forbidden on energy-conservation grounds. Thus the lowest-order process related to there being operators  $S_i^z$  in  $\mathcal{H}'_n$  is three-magnon scattering. In general, no restriction appears for three-magnon scattering other than the

fact that  $\hbar\omega_0 < \frac{1}{2}\hbar\omega_m$  to satisfy the  $\delta(E_k - E_{k'} - E_{k''} - \hbar\omega_n)$  requirement of Eq. (5.9). For the two-magnon or Raman-scattering process to take place, and a nuclear spin flip to occur, either a term of the form  $A_{yz}$  or  $D_{yz}$  which couples  $I^+$  to  $S_z$  must appear in  $\mathcal{H}'_n$  (i.e., the hyperfine +dipolar interaction tensor must be nondiagonal<sup>21</sup>) and/or the directions of quantization of the nuclear and electronic spin system must be noncollinear.

Returning to the hfs Hamiltonians appropriate to the  $^{19}\text{F}$  and  $^{55}\text{Mn}$  relaxation in  $\text{MnF}_2$  with  $\vec{H}_0 \parallel \hat{c}$ , and therefore the  $\hat{z}$  axis, the axis of quantization in both spin systems, we see from Eqs. (2.6) and (2.8) that

$$^{19}\mathcal{H}'_n = \sum_{i=1} (A_{yz}^i I_y S_z^i + A_{xx}^i I_x S_x^i + A_{yy}^i I_y S_y^i) + \sum_{i>4} D_{yz}^i I_y S_z^i, \quad (5.11)$$

$$^{55}\mathcal{H}'_n = ^{55}A_{xx} I_x S_x + ^{55}A_{yy} I_y S_y. \quad (5.12)$$

Thus only for  $^{19}(1/T_1)$  do we expect two-magnon contributions from the  $A_{yz}^i$  and  $D_{yz}^i$  terms, whereas none would be allowed for  $^{55}(1/T_1)$ . We now consider the explicit form of the  $^{19}\text{F}$  and  $^{55}\text{Mn}$  relaxation processes.

### 1. $^{19}\text{F}$ relaxation

a. *Two-magnon.* Using Eqs. (5.9) and (5.11) the Raman scattering from the 12 neighboring  $\text{Mn}^{2+}$  spins yields

$$\begin{aligned} ^{19} \left( \frac{1}{T_1} \right)_{\uparrow\uparrow} &= \frac{4\pi}{\hbar N^2} \sum_{\vec{k}, \vec{k}'} \{ [u_{\vec{k}}^2 u_{\vec{k}'}^2 \eta_{\vec{k}\uparrow\uparrow} (\eta_{\vec{k}\uparrow\uparrow} + 1) + v_{\vec{k}}^2 v_{\vec{k}'}^2 \eta_{\vec{k}\uparrow\uparrow} (\eta_{\vec{k}\uparrow\uparrow} + 1)] \\ &\times [(A_{yz}^I)^2 \sin^2(\vec{k} - \vec{k}') \cdot \frac{1}{2}(\vec{r}_I - \vec{r}_{I'}) + 4A_{yz}^I D_{yz}^{VI} \sin(\vec{k} - \vec{k}') \cdot \frac{1}{2}(\vec{r}_I - \vec{r}_I) \sin(\vec{k} - \vec{k}') \cdot \frac{1}{2}(\vec{r}_{VI'} - \vec{r}_{VI}) \\ &\times \cos(\vec{k} - \vec{k}') \cdot (\vec{r}_I - \vec{r}_{I'} - \vec{r}_{VI'} - \vec{r}_{VI})] + 2A_{yz}^I D_{yz}^{III} u_{\vec{k}} u_{\vec{k}'} v_{\vec{k}} v_{\vec{k}'} [\eta_{\vec{k}\uparrow\uparrow} (\eta_{\vec{k}\uparrow\uparrow} + 1) + \eta_{\vec{k}\uparrow\uparrow} (\eta_{\vec{k}\uparrow\uparrow} + 1)] \\ &\times [\sin(\vec{k} - \vec{k}') \cdot \frac{1}{2}(\vec{r}_{I'} - \vec{r}_I) \sin(\vec{k} - \vec{k}') \cdot \frac{1}{2}(\vec{r}_{III'} - \vec{r}_{III}) \\ &\times \cos(\vec{k} - \vec{k}') \cdot (\vec{r}_I - \vec{r}_{I'} - \vec{r}_{III'} - \vec{r}_{III})] + 2[\text{III} - \text{V}] \} \delta(E_{\vec{k}} - E_{\vec{k}'} - \hbar\omega_n). \end{aligned} \quad (5.13)$$

The notation  $[\text{III} - \text{V}]$  in the above means replace  $D_{yz}^{III}$  by  $D_{yz}^V$ ,  $\vec{r}_{III}$  by  $\vec{r}_V$ ,  $\vec{r}_{III'}$  by  $\vec{r}_{V'}$  in the previous term;  $\uparrow\uparrow$  is the same as used for designating frequencies in Eq. (2.7) and Bose factors in Eq. (2.8).

The dynamic relaxation probes the spectral density of the *square of the sum* of the local-field fluctuations at  $\omega_n$ . The significance then of the various cross terms which appear in Eq. (2.13) is that they represent the *interference* between contributions from different  $\text{Mn}^{2+}$  spins. For example, the term containing the factor

$$(A_{yz}^I)^2 \sin^2(\vec{k} - \vec{k}') \cdot (\vec{r}_I - \vec{r}_{I'})/2$$

takes cognizance of the fact that only the out-of-phase fluctuations of spins  $I$  and  $I'$  have a nonvanishing contribution to the local field induced by the off-diagonal elements of the  $A^I$  and  $A^{I'}$  hfs tensors, as was first noted in the earlier treatment<sup>10</sup> of  $^{19}(1/T_1)$  vs  $T$  at zero field. What was not considered before is the importance of cross terms connecting different spins through different coupling constants (e.g.,  $A_{yz}^I D_{yz}^{III}$ ). While it is true that, say,  $|D_{yz}^{III}| < |A_{yz}^I|$  the contributions that

the cross terms make to  $1/T_1$  are not as small as one usually surmises by cursorily comparing the separate autocorrelation contributions [i.e.,  $(D_{yz}^{II})^2$  with  $(A_{yz}^I)^2$ ]. Table II gives the location and magnitude of the coupling constants of the 12  $\text{Mn}^{2+}$  spins which were included in the two-magnon calculation above. Of course, other yet further removed  $\text{Mn}^{2+}$  spins will contribute to  $^{19}(1/T_1)$  but an order-of-magnitude estimate shows them not to contribute significantly. For example, even the term  $A_{yz}^I D_{yz}^{IV}$  is appreciably smaller than any of those included.

The composite results for the two-magnon calculation for  $^{19}(1/T_1)_{\uparrow}$  as a function of  $H_0$  at  $T = 4.2^\circ\text{K}$  are shown in Fig. 3 as the solid lines. The agreement between theory and experiment appears to be excellent over the entire field region except in the immediate vicinity of  $H_{\text{SF}}$ . In regards to the calculation certain details are of special interest. That part of the relaxation rate involving the coefficient  $(A_{yz}^I)^2$  and  $4A_{yz}^I D_{yz}^{VI}$  was calculated using the exact density of states as described in Appendix A. The numerical value of  $A_{yz}^I = 4.33 \times 10^{-4} \text{ cm}^{-1}$  that was chosen in the calculation is in excellent agreement with the value  $A_{yz}^I = (4.4 \pm 0.4) \times 10^{-4} \text{ cm}^{-1}$  obtained from EPR studies<sup>14</sup> of  $\text{Mn}^{2+}$  in  $\text{ZnF}_2$ —we shall return to a discussion of this point in a moment—and the  $D_{yz}^i$  are, of course, exact. However, for all other cross terms in Eq. (5.13) the small- $\vec{k}$  approximation to the density of states, suitably scaled, was used in the calculations. Since the latter terms contribute appreciably less to  $1/T_1$  than do the others it was felt that the requisite accuracy could be achieved within the framework of the small- $\vec{k}$  approximation. A discussion of the details of this and other approximations to the magnon density of states is given in Appendix A.

Perhaps what is most gratifying is to compare the different two-magnon contributions to  $^{19}(1/T_1)_{\uparrow}$  as a function of field at  $4.2^\circ\text{K}$ . This is done in Fig. 7 where the contributions from the  $(A_{yz}^I)^2$  and  $A_{yz}^I D_{yz}^i$  terms are separately given along with the total rate. Two things are to be noticed: (i) The cross terms  $A_{yz}^I D_{yz}^i$  have a measurably different field dependence from the  $(A_{yz}^I)^2$  terms; and (ii) the magnitude of the cross terms is such as to constitute an important correction to the over-all rate. This latter point relates to the earlier work<sup>10</sup> on  $^{19}(1/T_1)$  vs  $T$  at  $H_0 = 0$ . Since the cross terms were neglected the value of  $(A_{yz}^I)^2$  had to be made artificially larger than the experimental  $\text{Mn}^{2+}$  in  $\text{ZnF}_2$  measurement.<sup>14</sup> It is now clear that almost exact theoretical-experimental agreement is achieved with no adjustment of parameters by inclusion of these important cross terms.

The difference in the field dependence of

$^{19}(1/T_1)_{\uparrow}$  and  $^{19}(1/T_1)_{\downarrow}$  may be understood by just considering the  $(A_{yz}^I)^2$  term in Eq. (5.13) since, as shown in Fig. 7, its behavior dominates the relaxation rates. From Eq. (5.13) and Fig. 6 we see that when  $\eta_{\vec{k}\uparrow}$  is approximately the same as  $\eta_{\vec{k}\downarrow}$ , then the main contribution arises from the  $u_{\vec{k}\uparrow}^2 u_{\vec{k}\downarrow}^2$  part of the first term. This is the case near zero field and hence initially  $^{19}(1/T_1)_{\uparrow}$  decreases with  $H_0$  because  $\eta_{\vec{k}\uparrow}$  decreases with  $H_0$  and the converse holds for  $^{19}(1/T_1)_{\downarrow}$  and  $\eta_{\vec{k}\downarrow}$ . However, at low temperatures as  $H_0$  continues to increase  $\eta_{\vec{k}\downarrow} \gg \eta_{\vec{k}\uparrow}$ , particularly for the important small- $\vec{k}$  magnons and then the  $v_{\vec{k}\downarrow}^2 v_{\vec{k}\uparrow}^2 \eta_{\vec{k}\downarrow} (\eta_{\vec{k}\downarrow} + 1)$  term becomes appreciable, finally overcoming the initial field decreasing behavior of the  $^{19}(1/T_1)_{\uparrow}$  until it begins to increase with increasing field. Of course the  $u_{\vec{k}\uparrow}^2 u_{\vec{k}\downarrow}^2 \eta_{\vec{k}\downarrow} (\eta_{\vec{k}\downarrow} + 1)$  behavior of the  $^{19}(1/T_1)_{\downarrow}$  branch causes it to remain increasing with  $H_0$  for all fields.

b. *Three-magnon.* While it is most satisfying that quantitative agreement is found between experiment and two-magnon scattering theory over almost the entire region from  $H_0 = 0$  to  $H_D$ , it is less clear whether the rather abrupt increase in  $^{19}(1/T_1)_{\downarrow}$  near spin flop can be explained by residual odd-magnon scattering. Now three-magnon scattering should be the predominant mechanism for relaxation of the  $^{55}\text{Mn}$  nuclei, as indeed we will show to be the case. A rather complete theory of the latter, including second-order exchanged-enhanced processes,<sup>22</sup> has been developed by Freyne and Pincus.<sup>23</sup> We therefore adopt the following rationale: If three-magnon scattering,

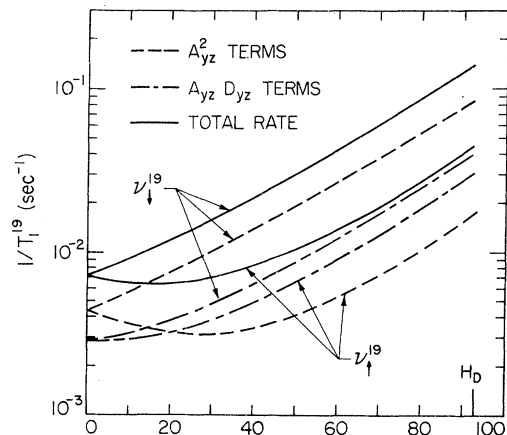


FIG. 7. Two-magnon theory for the  $^{19}\text{F}$  nuclear spin-lattice relaxation rate in  $\text{MnF}_2$  at  $4.2^\circ\text{K}$  as a function of  $\vec{H}_0 \parallel \hat{c}$ . The dashed curves (---) are the predicted rates for the two NMR branches including correlations only between type-I moments, whereas the curves (-·-·-) comprise the important hyperfine dipolar correlations as discussed in the text. The solid curve (—) shows the sum of these contributions.

which increases more rapidly with field than does the two-magnon process, is a contributing factor to the anomalous behavior of the  $^{19}\text{F}$  NSLR near  $H_D$  then, in principle, one should be able to "scale" the  $^{55}\text{Mn}$  and  $^{19}\text{F}$  rates in this region. However, before doing so it is necessary to investigate the importance of interference effects resulting from strong pair correlation between

neighboring spins on opposite sublattices, which is essential only in the  $^{19}\text{F}$  case.

Neglecting second-order exchange-enhanced processes, for which interference effects would be the same, the total three-magnon *hyperfine*-induced  $^{19}\text{F}$  NSLR, in the vicinity of  $H_D$ , is given by

$$\begin{aligned} \left(\frac{1}{T_1}\right)_\dagger &= \frac{\pi}{32\hbar N^3 S} \sum_{\vec{k}, \vec{k}', \vec{k}''} \eta_{\vec{k}}^\dagger \eta_{\vec{k}'}^\dagger (\eta_{\vec{k}''}^\dagger + 1) \{ 2(A_{xx}^I + A_{yy}^I)^2 u_{\vec{k}}^2 u_{\vec{k}'}^2 u_{\vec{k}''}^2 + (A_{xx}^{II} + A_{yy}^{II})^2 v_{\vec{k}}^2 v_{\vec{k}'}^2 v_{\vec{k}''}^2 \\ &+ 2(A_{xx}^I + A_{yy}^I)^2 u_{\vec{k}}^2 u_{\vec{k}'}^2 u_{\vec{k}''}^2 \cos(\vec{k}'' - \vec{k} - \vec{k}') \cdot (\vec{r}_I - \vec{r}_{I'}) \\ &- 2(A_{xx}^I + A_{yy}^I)(A_{xx}^{II} + A_{yy}^{II}) u_{\vec{k}}^\dagger u_{\vec{k}'}^\dagger u_{\vec{k}''}^\dagger v_{\vec{k}}^\dagger v_{\vec{k}'}^\dagger v_{\vec{k}''}^\dagger \\ &\times [\cos(\vec{k}'' - \vec{k} - \vec{k}') \cdot (\vec{r}_I - \vec{r}_{I'}) + \cos(\vec{k}'' - \vec{k} - \vec{k}') \cdot (\vec{r}_I - \vec{r}_{II})] \} \\ &\times \delta(E_{\vec{k}} + E_{\vec{k}'} - E_{\vec{k}''} - \hbar\omega_n). \end{aligned} \quad (5.14)$$

Here we have used the simplification that at a field sufficiently large, so that  $g\mu_B H_0 > kT$ , the relaxation will be dominated by terms which involve only Bose factors for the  $\vec{k}^\dagger$  magnon branch. Thus to obtain  $^{19}(1/T_1)_\dagger$  it is necessary to simply interchange  $u_{\vec{k}}$  and  $v_{\vec{k}}$  in the last equation.

The first two terms in Eq. (2.14) represent relaxation of a  $^{19}\text{F}$  moment caused by the three adjacent  $\text{Mn}^{2+}$  spins in the absence of interference effects, whereas the third term explicitly exhibits the interference between spins I and I'. The positive coefficient of the latter term represents the fact that, for small- $\vec{k}$  excitations,  $\text{Mn}^{2+}$  spins I and I' fluctuate in phase.

The most important feature of Eq. (5.14) is the negative sign of the last term and is directly traceable to the negative sign preceding the  $v_{\vec{k}}$ 's in the transformation to normal mode operators [see Eq. (5.3)] and that *odd* numbers of  $v_{\vec{k}}$ 's appear as coefficients in Eq. (2.14). The physical interpretation to be attributed to this is that for small- $\vec{k}$  excitations  $\text{Mn}^{2+}$  spins I and I' fluctuate opposite in phase to the type-II spins. This by itself would not be decisive were it not for the fact that

$(A_{xx}^{II} + A_{yy}^{II}) > (A_{xx}^I + A_{yy}^I)$  and hence the degree of cancellation of the first three terms by the last term could be significant. Moreover, since one must interchange  $u_{\vec{k}}$  with  $v_{\vec{k}}$  in going from the expression for  $^{19}(1/T_1)_\dagger$  to  $^{19}(1/T_1)_\dagger$ , the relative weighting of the various auto- and pair-correlation terms will change and with it the relative degree of cancellation to be expected. As mentioned above, rather than numerically calculating the three-magnon scattering for the  $^{19}\text{F}$  NSLR we will make use of the  $^{55}\text{Mn}$  experimental results to "scale" the expected contribution to  $^{19}(1/T_1)_\dagger$  and  $^{19}(1/T_1)_\dagger$  from this process, but explicitly taking into account the different contributions that the cross terms make to the two  $^{19}\text{F}$  NSLR rates. We will see by doing this we can explain most of the observed difference in the magnitudes of the two rates in the region of field close to  $H_{SF}$ .

## 2. $^{55}\text{Mn}$ relaxation: Three magnon

Using the transverse Hamiltonian of Eq. (5.12), with  $A_{xx} = A_{yy} = A$ , the first-order three-magnon-induced  $^{55}\text{Mn}$  NSLR rate has the form

$$\begin{aligned} \left(\frac{1}{T_1}\right)_\dagger &= \frac{\pi A^2}{8\hbar S N^3} \sum_{\vec{k}, \vec{k}', \vec{k}''} [u_{\vec{k}}^2 u_{\vec{k}'}^2 u_{\vec{k}''}^2 \eta_{\vec{k}}^\dagger \eta_{\vec{k}'}^\dagger (\eta_{\vec{k}''}^\dagger + 1) + v_{\vec{k}}^2 v_{\vec{k}'}^2 v_{\vec{k}''}^2 \eta_{\vec{k}}^\dagger \eta_{\vec{k}'}^\dagger (\eta_{\vec{k}''}^\dagger + 1) \\ &+ 4v_{\vec{k}}^2 u_{\vec{k}'}^2 u_{\vec{k}''}^2 \eta_{\vec{k}}^\dagger \eta_{\vec{k}'}^\dagger (\eta_{\vec{k}''}^\dagger + 1) + 4v_{\vec{k}}^2 u_{\vec{k}}^2 v_{\vec{k}'}^2 \eta_{\vec{k}}^\dagger \eta_{\vec{k}'}^\dagger (\eta_{\vec{k}''}^\dagger + 1)] \delta(E_{\vec{k}} + E_{\vec{k}'} - E_{\vec{k}''} - \hbar\omega_n). \end{aligned} \quad (5.15)$$

To obtain  $^{55}(1/T_1)_\dagger$ , it is simply necessary to interchange  $u_{\vec{k}}$  and  $v_{\vec{k}}$  in the above equation. It may be seen from the above that at low temperatures and at fields that are very large the term proportional to  $u_{\vec{k}}^2 u_{\vec{k}'}^2 u_{\vec{k}''}^2$  will dominate  $^{55}(1/T_1)_\dagger$ . Hence there

will be a rapidly increasing dependence of  $^{55}(1/T_1)_\dagger$  on  $H_0$  arising from the product of Bose factors  $\eta_{\vec{k}}^\dagger \eta_{\vec{k}'}^\dagger (\eta_{\vec{k}''}^\dagger + 1)$ . Likewise,  $^{55}(1/T_1)_\dagger$  will increase rapidly with field at high fields. Moreover, if this first term was the sole contribution, and we as-

sume that  $u_{\vec{k}}^2 \approx u_0^2$  and  $v_{\vec{k}}^2 \approx v_0^2$  for all  $\vec{k}, \vec{k}'$  and  $\vec{k}''$ , then we would expect that at high fields and low  $T$

$${}^{55}\left(\frac{1}{T_1}\right)_{\uparrow} / {}^{55}\left(\frac{1}{T_1}\right)_{\downarrow} \simeq \left(\frac{u_0^2}{v_0^2}\right)^3 \approx 2.9, \quad (5.16)$$

which, as can be seen from Fig. 4, is close to what is observed:

$${}^{55}\left(\frac{1}{T_1}\right)_{\uparrow} / {}^{55}\left(\frac{1}{T_1}\right)_{\downarrow} \simeq 2.5.$$

We have not calculated the actual field dependence predicted by Eq. (2.15) because it is clear from the work of others<sup>22-25</sup> that second-order processes enhance the three-magnon rate obtained from the noninteracting theory. Freyne and Pincus<sup>23</sup> have in fact made such a calculation including all processes in which a virtual magnon is created by the nuclear spin flip and then subsequently scattered via the dynamical magnon-magnon interaction involving the transverse parts of the exchange Hamiltonian. Their calculation uses the small- $\vec{k}$  approximation for the magnon density of states and also makes certain simplifications in averaging over some scalar products of the scattered-magnon wave vectors. The results of their theory *multiplied by a factor of  $\frac{1}{2}$*  are shown in Fig. 4 as the solid lines (see Fig. 4 caption). Although there is a clear indication in the theory of the strong field dependence found in the experimental result it is also obvious that the Freyne-Pincus result overestimates the rates by about a factor of 2. The agreement is remarkably good over most of the field range again, except in the vicinity of  $H_D$ , where  ${}^{55}(1/T_1)_{\uparrow}$  and  ${}^{55}(1/T_1)_{\downarrow}$  both increase more rapidly than the three-magnon theory predicts.

Since the calculation produces a result that is *larger* than is observed and yet neglected higher-order processes would only *add* to the calculated rate we suggest that the theoretical result is in error. Support for this contention comes from comparing the three-magnon exchange enhancement at  $H_0 = 0$  first calculated by Beeman and Pincus<sup>22</sup> with the result obtained by Harris.<sup>25</sup> The latter author used the Dyson-Maleev transformation to boson operators rather than the Holstein-Primakoff one. Beeman and Pincus found an enhancement of 2.05, Harris an enhancement of 2.0, while Freyne and Pincus now find the enhancement to be 3.6. We also suspect that this *enhancement* of the three-magnon rate does not depend strongly on field; otherwise, the relation given in Eq. (5.16) would not hold. Unfortunately no calculation was made of the ratio of the enhanced to the unenhanced rates as a function of  $H_0$ .

Putting aside these rather small differences between theory and experiment, we should emphasize two points: (a) the observed rapid vari-

ation of  ${}^{55}(1/T_1)_{\uparrow}$  with  $H_0$  due to three-magnon scattering is substantiated by the theory and (b) the observed divergent behavior as  $H_0$  approaches  $H_{SF}$  is not given by existing theories. We now turn to the latter in attempting to understand both the  $^{19}\text{F}$  and  $^{55}\text{Mn}$  NSLR rates in the region  $H_{SF} - H_0 \ll H_{SF}$ .

### 3. Relaxation near spin flop

It is apparent that, despite the rather good agreement between experiment and theory for both the  $^{19}\text{F}$  and  $^{55}\text{Mn}$  rates well below the region of spin-flop, low-order perturbation theory does not suffice to describe the increasingly rapid rates as  $H_0$  approaches  $H_{SF}$ . We will show in this section that (i) the difference in the behavior of  ${}^{19}(1/T_1)_{\uparrow}$  and  ${}^{19}(1/T_1)_{\downarrow}$  in the immediate vicinity of  $H_D$  is mainly explained in terms of transverse fluctuations of the  $\text{Mn}^{2+}$  spins, using the observed  $^{55}\text{Mn}$  NSLR rates and the known hfs couplings to scale  ${}^{19}(1/T_1)$  to  ${}^{55}(1/T_1)$  and, (ii) the observed  $(H_{SF} - H_0)^{-3/2}$  behavior of  ${}^{55}(1/T_1)_{\uparrow}$  is directly obtained from a "one-magnon" phenomenological theory in which the magnon lifetime  $\Gamma_{\vec{k}}$  at low temperatures is assumed to depend strongly on  $T$  but weakly on  $\vec{k}$  and  $H_0$  for those small- $\vec{k}$  magnons that are important to the NSLR. We shall refer to the behavior of the  $^{19}\text{F}$  and  $^{55}\text{Mn}$  rates in this high-field region as "anomalous" to distinguish them from what we consider to be the first-principles explanation of the rates in the region well away from  $H_{SF}$ .

*a. Anomalous  $^{19}\text{F}$  NSLR.* An alternate description<sup>26</sup> of NSLR is obtained in terms of the appropriate spin-correlation functions. For example, in the case of the  $^{55}\text{Mn}$  NMR where only transverse fluctuations of  $\vec{S}$  may contribute to  ${}^{55}(1/T_1)$  we may write Eq. (5.15) as

$${}^{55}\left(\frac{1}{T_1}\right)_{\downarrow} = \frac{1}{2} \left(\frac{2A}{2\hbar}\right)^2 \int_{-\infty}^{\infty} \langle \{S_{\downarrow}^{\dagger}(t)S_{\downarrow}^{\dagger}(0)\} \rangle \cos \omega_n t dt. \quad (5.17a)$$

The arrows represent the direction of the electronic moments with respect to  $\vec{H}_0$ , the  $\langle \rangle$  indicates an ensemble average and the  $\{ \}$  an indication of a symmetrization of the operators. In this sense the  $^{55}\text{Mn}$  NSLR is a measure of the spectral density of the transverse electronic spin fluctuations at  $\omega = \omega_n$  with  ${}^{55}(1/T_1)_{\downarrow}$  and  ${}^{55}(1/T_1)_{\uparrow}$  separately sensing those fluctuations on the two different sublattices. The three-magnon relaxation then is the lowest-order contribution to the Fourier transform of the autocorrelation function given in Eq. (5.17a).

For simplicity we rewrite Eq. (5.17a) as

$${}^{55}\left(\frac{1}{T_1}\right)_{\downarrow} = (2^{55}A)^2 \bar{S}_{\downarrow}(H, T) = (2^{55}A)^2 \bar{S}_{\downarrow}, \quad (5.17b)$$

where, in the latter, we drop the implicit dependence of  $\bar{S}_{\downarrow}$  on  $H$  and  $T$ , and define

$$\bar{S}_{\downarrow} \equiv \frac{1}{8\hbar^2} \int_{-\infty}^{\infty} \langle \{S_{\downarrow}^{\dagger}(t)S_{\downarrow}^{\dagger}(0)\} \rangle \cos \omega_n t dt. \quad (5.18)$$

Clearly the power spectrum of the fluctuations sensed by the  ${}^{19}\text{F}$  nuclei will involve similar correlation functions, particularly if the anomalous behavior near  $H_D$  arises from transverse spin fluctuations. However, pair correlation is very important to the  ${}^{19}\text{F}$  NSLR because of the cross coupling of a given  ${}^{19}\text{F}$  nucleus to its various neighbors. We generalize (5.18) to include, for example,

$$\bar{S}_{\uparrow\uparrow\uparrow} \equiv \frac{1}{8\hbar^2} \int_{-\infty}^{\infty} \langle \{S_{\uparrow}^{\dagger}(t)S_{\uparrow}^{\dagger}(0)\} \rangle \cos \omega_n t dt. \quad (5.19)$$

Certain of the  $\bar{S}$  are identical and we simplify Eq. (5.19) further by writing

$$\begin{aligned} \bar{S}_{\uparrow\uparrow\uparrow} &\equiv \bar{S}^{\uparrow}; & \bar{S}_{\uparrow\uparrow\downarrow} &\equiv \bar{S}^{\uparrow\downarrow}; \\ \bar{S}_{\uparrow\downarrow\uparrow} &\equiv \bar{S}^{\uparrow\downarrow}, & \bar{S}_{\downarrow\uparrow\uparrow} &\equiv \bar{S}^{\downarrow\uparrow}, \end{aligned} \quad (5.20)$$

where  $a$  and  $b$  denote auto- and pair-correlation functions, respectively. Thus both the  ${}^{55}\text{Mn}$  and  ${}^{19}\text{F}$  relaxations that arise from *transverse fluctuations* may be quite simply expressed as

$${}^{55}\left(\frac{1}{T_1}\right)_{\uparrow} = (2^{55}A)^2 \bar{S}^{\uparrow}, \quad {}^{55}\left(\frac{1}{T_1}\right)_{\downarrow} = (2^{55}A)^2 \bar{S}^{\downarrow}; \quad (5.21)$$

$$\begin{aligned} {}^{19}\left(\frac{1}{T_1}\right)_{\uparrow} &= 2(A_{xx}^I + A_{yy}^I)^2 \bar{S}^{\uparrow} + (A_{xx}^{II} + A_{yy}^{II})^2 \bar{S}^{\uparrow} \\ &+ 2(A_{xx}^I + A_{yy}^I)^2 \bar{S}^{\uparrow\downarrow} + 4(A_{xx}^I + A_{yy}^I)(A_{xx}^{II} + A_{yy}^{II}) \bar{S}^{\uparrow\downarrow}; \end{aligned} \quad (5.22)$$

$$\begin{aligned} {}^{19}(1/T_1)_{\downarrow} &= 2(A_{xx}^I + A_{yy}^I)^2 \bar{S}^{\downarrow} \\ &+ (A_{xx}^{II} + A_{yy}^{II})^2 \bar{S}^{\downarrow} + 2(A_{xx}^I + A_{yy}^I) \bar{S}^{\downarrow} \\ &+ 4(A_{xx}^I + A_{yy}^I)(A_{xx}^{II} + A_{yy}^{II}) \bar{S}^{\downarrow}. \end{aligned} \quad (5.23)$$

If the  ${}^{19}\text{F}$  NSLR only depended on  $\bar{S}^a$  the scaling that would be required would be simple. Clearly some assumptions must be made to relate the unknown  $\bar{S}^b$  to the  $\bar{S}^a$ . At low temperatures, for all values of  $H_0$ , the magnons involved in the relaxation are of small  $|\vec{k}|$  (see Appendix A.) It is not unreasonable in this case then to assume that the pair-correlation function has the same field dependence as does the autocorrelation function for spins on the *same* sublattice, i.e.,

$$\bar{S}^b = \alpha \bar{S}^a; \quad \bar{S}^{\downarrow} = \alpha \bar{S}^{\uparrow}, \quad (5.24)$$

with  $\alpha$  independent of  $H_0$  at a fixed  $T$ .

In the three-magnon scattering [see Eq. (5.14)] this implies that one is assuming  $u_{\vec{k}}^{\uparrow}$  and  $v_{\vec{k}}^{\uparrow}$  and the phase factors  $\cos(\vec{k}'' - \vec{k} - \vec{k}') \cdot (\vec{r}_1 - \vec{r}_1')$ , etc., do not vary strongly with  $\vec{k}$  at small  $\vec{k}$ .

The second assumption concerns the relation between  $\bar{S}_{\downarrow}^a$  and  $\bar{S}_{\downarrow}^b$ . We have noted that over most of the region of field the measured ratio of

$${}^{55}(1/T_1)_{\uparrow} / {}^{55}(1/T_1)_{\downarrow}$$

is roughly constant. This is particularly true in the vicinity of  $H_{\text{SF}}$  where, despite the fact that both are strong functions of field, their ratio is constant; therefore we take, using Eq. (5.21),

$$\bar{S}_{\downarrow}^b = \Delta \bar{S}_{\downarrow}^a, \quad (5.25)$$

with  $\Delta$  independent of  $H_0$  at a fixed  $T$ . It is experimentally observed that  $\Delta = 0.4$ . We remarked earlier that this is related to the fact that at high fields, in particular, the dominant excitations are all on one-magnon branch, and in the three-magnon-scattering theory  $\Delta$  is given by the ratio  $u_{\vec{k}}^6/v_{\vec{k}}^6$ . [See Eq. (5.16).]

Since we have shown it to be plausible that one may neglect the field dependence, if any, of  $\bar{S}_{\uparrow}^b/\bar{S}_{\uparrow}^a$  as well as  $\bar{S}_{\downarrow}^b/\bar{S}_{\downarrow}^a$ , it is not unreasonable to assume that  $\bar{S}_{\uparrow\downarrow}^b/\bar{S}_{\uparrow\downarrow}^a$  is also field independent at a fixed  $T$ , at least in the narrow high-field region  $H_{\text{SF}} - H_0 \ll H_{\text{SF}}$ . Thus we take

$$\bar{S}_{\uparrow\downarrow}^b = \beta \bar{S}_{\uparrow\downarrow}^a = \beta \Delta \bar{S}_{\uparrow\downarrow}^a. \quad (5.26)$$

The physically allowable range of values for the undetermined parameter  $\alpha$  is  $0 < \alpha < 1$ . To see what might be the bounds on  $\beta$  we substitute the definitions Eqs. (5.24)–(5.26) into Eqs. (5.21)–(5.23) and obtain the two algebraic equations, using  $A_I \equiv A_{xx}^I + A_{yy}^I$  and  $A_{II} \equiv A_{xx}^{II} + A_{yy}^{II}$ ,

$$\begin{aligned} R_{\uparrow} &\equiv \left(\frac{1}{T_1}\right)_{\uparrow} / \left(\frac{1}{T_1}\right)_{\downarrow} \\ &= \frac{1}{(2^{55}A)^2} (2A_I^2 + A_{II}^2/\Delta + 2\alpha A_I^2 - 4\beta A_I A_{II}), \end{aligned} \quad (5.27)$$

$$\begin{aligned} R_{\downarrow} &\equiv \left(\frac{1}{T_1}\right)_{\downarrow} / \left(\frac{1}{T_1}\right)_{\uparrow} \\ &= \frac{1}{(2^{55}A)^2} (2A_I^2 + \Delta A_{II}^2 + 2\alpha A_I^2 - 4\Delta\beta A_I A_{II}). \end{aligned} \quad (5.28)$$

Then  $\beta$  must be restricted to the values

$$0 < \beta < \frac{2A_I^2 + (1/\Delta)A_{II}^2 + 2\alpha A_I^2}{4A_I A_{II}},$$

with the upper limit corresponding to the point at which exact cancellation occurs in Eq. (5.14) for  ${}^{19}(1/T_1)_{\uparrow}$ . In the region of small- $\vec{k}$  excitations one, in fact, expects  $\beta$  to be close to this upper limit,  $\beta = 1.58$  if  $\alpha = 1$ .

It is possible to estimate  $\beta$  from spin-wave theory. In general for all odd  $N$ -magnon processes which are dominated by the downgoing magnon branch it is found, in the small- $\vec{k}$  approximation, that

$$\bar{S}_\uparrow^a / \bar{S}_\downarrow^a \approx 1/\Delta \approx (u_0/v_0)^{2N}$$

and  $\beta \approx (u_0/v_0)^N$  is therefore given by  $\beta = (1/\Delta)^{1/2}$ . A particular example of this relationship between  $\beta$  and  $\Delta$  for  $N=3$  may be seen in Eq. (5.15). Moreover, the experimentally observed values of  $1/\Delta = 2.5$  and  $\beta = 1.6$  are consistent with the values of  $u_{\vec{k}}$  and  $v_{\vec{k}}$  near  $\vec{k}=0$ . In Fig. 8 we plot the quantities  $1/R_\uparrow$  and  $1/R_\downarrow$  as a function of  $\beta$  for the value  $\alpha = 1$ . The choice of the latter parameter value is in keeping with the fact that, if we interpret  $\alpha$  within the spin-wave theory, it is proportional to a  $\cos\vec{k} \cdot (\vec{\tau}_1 - \vec{\tau}_{1'})$  factor which, in the small- $\vec{k}$  approximation, will be close to unity. One sees that for values of  $\beta$  larger than 1.5,  $1/R_\uparrow$  rapidly becomes much greater than  $1/R_\downarrow$ . The value  $\beta \approx 1.54$ , where  $1/R_\uparrow$  is equal to the experimentally determined ratio, is in qualitative agreement with the estimate given above. If Eqs. (5.27) and (5.28) gave an exact description of the anomalous contributions to the  $^{19}\text{F}$  NSLR from transverse fluctuations, then  $1/R_\downarrow$  would also intersect the corresponding experimental ratio at the same value of  $\beta$ . Before considering why the simple theory might not give a precise description of the anomalous rates, we should emphasize that it clearly shows that the cross terms contained in the theory for the transverse fluctuations *do* account for most of the magnitude of the anomalous rates and, in particular, that the NSLR rate of the  $^{19}\nu_\uparrow$  branch can be much smaller than the corresponding  $^{19}\nu_\downarrow$  one.

We have considered how the inclusion of diagonal dipolar terms (e.g.,  $A_{xx}^I D_{xx}^{III}$ ) might modify the above conclusion and find that, at most, they would result in only slightly different values of  $\beta$  being obtained for the observed  $\Delta$  and physically plausible value of  $\alpha \approx 1$ .

The two lines  $(1/R)_\downarrow(\text{expt})$  and  $(1/R)_\uparrow(\text{expt})$  shown in Fig. 8 presume that *all* of the anomalous contribution to the  $^{19}\text{F}$  NSLR rate results from *transverse* fluctuations. If indeed part of the anomalous behavior was caused by *longitudinal* fluctuations—not obtainable from the simple two-magnon-scattering theory—then both values of  $(1/R)(\text{expt})$  should be increased. For example, if we assume longitudinal fluctuation contributes 40% of the anomalous relaxation on both branches, then, as may be seen from the dashed lines, the curves for  $(1/R)_\uparrow$  and  $(1/R)_\downarrow$  will intersect the two dashed lines at the same value of  $\beta$ . In actual fact, second-order contributions to the  $^{19}\text{F}$  NSLR do exist

which arise from longitudinal fluctuations of the electronic spins. In particular a four-magnon process exists in which a thermal magnon scatters from a nuclear spin [via the term  $A_{yz}I_y S_z$  in Eq. (5.11)] emitting a virtual magnon which in turn interacts with a second thermal magnon via four-magnon exchange scattering.<sup>27</sup> Thus this process is similar to the three-magnon exchange enhanced processes discussed above.

Although it is straightforward to show that four-magnon processes are negligible at  $H_0=0$ ,<sup>28</sup> the very strong field dependence arising from four Bose factors could make these processes important enough near spin-flop to explain some of the residual anomalous behavior of  $^{19}(1/T_1)_\downarrow$ .

One further result is pertinent to the anomalous contribution to  $^{19}(1/T_1)_\downarrow$ . We have made some qualitative measurements at high fields of  $^{19}(1/T_1)_\downarrow$  at  $T=5.8$  and  $7.8$  °K. At a fixed  $H_0$  in the vicinity of  $H_{\text{SF}}$ , it appears that the anomalous contribution to  $^{19}(1/T_1)_\downarrow$ , over and above what is calculated

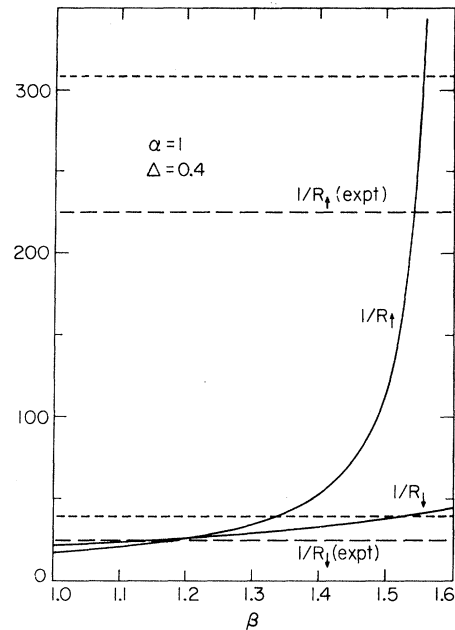


FIG. 8. Ratio of the  $^{19}\text{F}$  and  $^{55}\text{Mn}$  relaxation times  $1/R_\uparrow \equiv ({}^{19}T_{1\uparrow}/{}^{55}T_{1\uparrow})_{H,T}$  and  $1/R_\downarrow \equiv ({}^{19}T_{1\downarrow}/{}^{55}T_{1\downarrow})_{H,T}$  calculated from a phenomenological theory which utilizes the two interference parameters  $\alpha$  and  $\beta$  and the experimentally determined ratio  $\Delta = ({}^{55}T_{1\uparrow}/{}^{55}T_{1\downarrow})_{H,T}$ . For  $T=4.2$  °K and  $H_0=92.3$  kOe the calculated curves (solid lines) are compared as a function of  $\beta$  with measured values (long dashes) of the ratios  $1/R_\uparrow$  and  $1/R_\downarrow$ . The short dashed lines result for  $1/R(\text{expt})$  if it is assumed that only 60% of the anomalous part of the measured values of  $^{19}(1/T_1)_{\uparrow\downarrow}$  arise from transverse fluctuations. The latter lines represent a solution of Eqs. (5.27) and (5.28) which is self-consistent.

from the two-magnon-scattering theory, increases as  $T^n$  with  $3 < n < 5$ . Since the two-magnon contribution increases more rapidly with  $T$  it is clear that the anomalous part of  $^{19}(1/T_1)_\dagger$  will be submerged at higher temperatures. Concerning the rough temperature dependence found for  $^{19}(1/T_1)_\dagger$ , we will have some further comments to make in connection with the direct processes involved in the scattering of damped magnons.

b. Anomalous  $^{55}\text{Mn}$  NSLR—"one-magnon" scattering. The experimental data shown in Fig. 9 are plotted in a fashion that emphasizes the discrepancy between the three-magnon theory, including exchange-enhanced scattering, and the observed results in the field region  $(H_{\text{SF}} - H_0) \ll H_{\text{SF}}$ . Exhibiting the data in a  $\ln^{55}(1/T_1)$  vs  $\ln(H_{\text{SF}} - H_0)$  plot points up an interesting feature of the NSLR; namely,  $^{55}(1/T_1)$  diverges as  $(H_{\text{SF}} - H_0)^{-3/2}$  at 4.2 °K! This behavior is simply not obtained from the low-order magnon perturbation theory for the transverse fluctuating fields.

One might regard this as a deficiency of the spin-wave theory in the field region where  $E_{\vec{k}\dagger} \rightarrow 0$ , for  $\vec{k} = 0$ , as  $H_0 \rightarrow H_{\text{SF}}$ —which it certainly is—or as evidence for some precursor criticallylike fluctuations associated with the spin-flop instability. Indeed, either or both of these premises may be correct but it is not obvious how one rigorously takes them into account within the present theories.

However, we would like to suggest how, from a phenomenological point of view, one might interpret the  $(H_{\text{SF}} - H_0)^{-3/2}$  behavior in the context of "one-magnon" scattering involving damped spin waves. Turov has shown<sup>29</sup> that if magnon damping is associated with interactions of magnons, either with each other, the lattice or impurities, then one may express the NSLR in *ferromagnets* in terms of a "one-magnon" process as

$$\frac{1}{T_1} = \left(\frac{A}{\hbar}\right)^2 \frac{S}{N} \sum_{\vec{k}} \frac{(1 + 2\eta_{\vec{k}}) \Gamma_{\vec{k}}(\omega_n)}{(\omega_{\vec{k}} - \omega_n)^2 + \Gamma_{\vec{k}}^2(\omega_n)} \quad (5.29)$$

where  $\Gamma_{\vec{k}}(\omega_n)$  is a quantity which characterizes the magnon damping at  $\omega = \omega_n$ . Recalling that in the linear theory for the direct process, the  $\vec{k}$  summation contains

$$\sum_{\vec{k}} (1 + 2\eta_{\vec{k}}) \delta(\hbar\omega_{\vec{k}} - \hbar\omega_n),$$

we may regard the factor

$$\Gamma_{\vec{k}}(\omega_n) / [(\omega_{\vec{k}} - \omega_n)^2 + \Gamma_{\vec{k}}^2(\omega_n)]$$

as the magnon spectral weight of wave vector  $\vec{k}$  at the energy  $\hbar\omega_n$ .

For an antiferromagnet at low temperatures and at fields close to spin flop the thermal excitations

on the low-energy branch are similar in many ways to a ferromagnet in a field with a small anisotropy gap. Generalizing Eq. (2.29) to the *antiferromagnetic* case, we find

$$^{55} \left( \frac{1}{T_1} \right)_{\dagger} = \left( \frac{A}{\hbar} \right)^2 \frac{S}{N} \sum_{\vec{k}} \frac{(1 + 2\eta_{\vec{k}}) u_{\vec{k}}^2 \Gamma_{\vec{k}\dagger}(\omega_n)}{(\omega_{\vec{k}} - \omega_n)^2 + \Gamma_{\vec{k}}^2(\omega_n)}. \quad (5.30)$$

For  $^{55}(1/T_1)_\dagger$  one should substitute  $v_{\vec{k}}^2$  for  $u_{\vec{k}}^2$ . Since, except for fields very close to spin flop, we would expect  $\omega_{\vec{k}\dagger} \gg \Gamma_{\vec{k}\dagger}(\omega_n)$  at low temperatures and  $\omega_{\vec{k}} \gg \omega_n$ , then

$$^{55} \left( \frac{1}{T_1} \right)_{\dagger} \approx A^2 \frac{S}{N} \sum_{\vec{k}} \frac{(1 + 2\eta_{\vec{k}}) u_{\vec{k}}^2 \Gamma_{\vec{k}\dagger}(\omega_n)}{\gamma^2 [(H_{\text{SF}}^2 + b^2 \vec{k}^2)^{1/2} - H_0]^2}. \quad (5.31)$$

If we assume for the moment that  $\Gamma_{\vec{k}\dagger}(\omega_n)$  depends strongly on  $T$  but is independent of  $\vec{k}$  over the range of  $\vec{k}$ 's of interest at low temperatures and also independent of  $H_0$  in the region  $H_{\text{SF}} - H_0 \ll H_{\text{SF}}$ , then one may easily calculate  $^{55}(1/T_1)_\dagger$ . In partic-

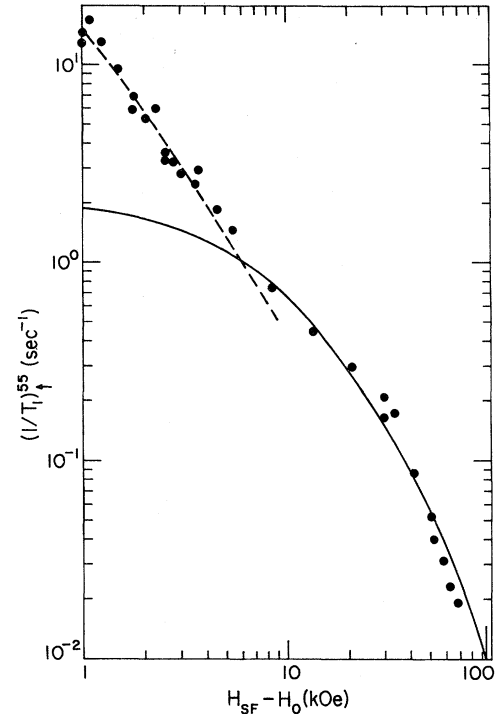


FIG. 9. Nuclear spin-lattice relaxation rate for the  $^{55}\text{Mn}$  ( $^{55}\nu_\dagger$  branch) in  $\text{MnF}_2$  at 4.2 °K as a function of the distance  $(H_{\text{SF}} - H_0)$  from the spin-flop transition. The solid line is the adjusted prediction of the Freyre-Pincus three-magnon theory (see Fig. 4) and the dashed line is the result of a one-magnon calculation where in the latter the lifetime of the magnons is included. The parameter  $\Gamma_{\vec{k}}(\omega_n) = 1.8 \times 10^6 \text{ sec}^{-1}$  was used to characterize this lifetime effect.

ular, for  $\hbar\omega_0 \ll kT$ , it is simple to show that for  $H_{\text{SF}} - H_0 \ll H_{\text{SF}}$ ,

$$\frac{1}{T_1} \propto \frac{1}{(H_{\text{SF}} - H_0)^{3/2}}. \quad (5.32)$$

The upper curve in Fig. 9 at small values of  $H_{\text{SF}} - H_0$  is the result of a calculation of Eq. (5.31) with the value  $\Gamma_{\vec{k}\uparrow}(\omega_n) = 1.8 \times 10^6 \text{ sec}^{-1}$  chosen to best fit the data.

Several remarks are in order concerning the above results: (a) As Turov<sup>29</sup> has emphasized one should *not* regard  $\Gamma_{\vec{k}}(\omega_n)$  as the spin-wave lifetime as derived from measurements such as antiferromagnetic resonance. (b) It is not clear whether one should add these results on to the exchange-enhanced part of the three-magnon theory or not, since the latter purports to include lifetime broadening of the magnons.<sup>30</sup> (c) One might expect that  $\Gamma_{\vec{k}}$  would be a strong function of  $\vec{k}$  and  $H_0$  even for the small- $\vec{k}$  magnons. Nevertheless, parallel pumping measurements<sup>31</sup> in antiferromagnetic  $\text{CuCl}_2 \cdot 2\text{H}_2\text{O}$  at low temperatures support the approximation that the spin-wave lifetimes for the small- $\vec{k}$  magnons become increasingly field *independent* as well as  $\vec{k}$  independent as  $T$  becomes much smaller than  $T_n$ . It might also be mentioned that the value of  $\Gamma_{\vec{k}}(\omega_n)$  that is found from our analysis is not unreasonable when compared with the spin-wave lifetimes  $\Gamma_{\vec{k}}^{-1} \approx 10^{-6} \text{ sec}$  that have been obtained in interpreting the  $\text{MnF}_2$  AFMR experiments at high field<sup>9</sup>. (d) Measurements of the spin-wave lifetimes in the parallel pumping experiments in  $\text{CuCl}_2 \cdot 2\text{H}_2\text{O}$ ,<sup>31</sup> and the four-magnon-scattering contribution to the antiferromagnetic-resonance (AFMR) linewidth in  $\text{MnF}_2$  at high fields<sup>32</sup> as a function of temperature, show an approximate  $T^4$  behavior. Again keeping in mind comment (a) above, it still would suggest that  $^{55}(1/T_1)_{\uparrow\downarrow}$  should vary as  $T^5$  in the region  $g\mu_B(H_{\text{SF}} - H_0) \ll kT$ . We have not made measurements of the  $^{55}(1/T_1)$  in this temperature region but, as remarked at the end of Sec. IV, we did find an approximate  $T^n$  behavior with  $3 < n < 5$ , to the anomalous contribution to  $^{19}(1/T_1)_{\uparrow}$ . Measurements of  $^{55}(1/T_1)_{\uparrow\downarrow}$  as a function of temperature in the high-field region are now in progress by one of the authors (A.R.K.) in collaboration with Dr. J-P. Boucher. From these results and a more complete treatment of all magnon-scattering processes, direct and induced, we hope to resolve the question of the origin of the divergence of  $^{55}(1/T_1)$  as  $H_0 \rightarrow H_{\text{SF}}$ .

It should be pointed out that for  $\text{MnF}_2$  at 4.2 °K, Eq. (5.31) not only leads to the proportionality (5.32), but it also predicts that  $^{55}(1/T_1)_{\uparrow\downarrow} / ^{55}(1/T_1)_{\uparrow} \cong u_0^2/v_0^2 = 1.4$ . Experimentally we find  $^{55}(1/T_1)_{\uparrow\downarrow} / ^{55}(1/T_1)_{\uparrow} = 2.5$  for  $(H_{\text{SF}} - H_0) \lesssim 10 \text{ kOe}$ .

Nevertheless our phenomenological approach gives an indication that perhaps spin-wave damping may be an important consideration in calculations of the NSLR near spin flop and, moreover, that the NSLR is an extremely sensitive probe of relatively small values of spin-wave lifetime broadening.

### C. rf-field enhancements and the divergence of $\chi_{\perp}$

The enhancement of the rf field experienced by the nuclei in the walls and domains of a ferromagnet is a subject which has received much attention since the pioneering work of Portis and Gossard.<sup>33</sup> We show now by analogy with domain-rotation enhancement in ferromagnets that the NMR signal in antiferromagnets also will be appreciably enhanced as  $H_0$  approaches  $H_{\text{SF}}$  because of the divergence of  $\chi_{\perp}$ .

In a saturated uniaxial *ferromagnet* with  $\vec{H}_0 \parallel \hat{c}$ , and anisotropy field  $H_A$  the enhancement  $\eta^{\parallel}$  for  $\vec{H}_{\text{rf}} \perp \hat{c} \parallel \hat{z}$  is<sup>34</sup>

$$\text{ferro: } \eta^{\parallel} = \frac{H_n}{H_m} = \frac{H_n}{H_0^{\parallel} + H_A + (H_D^{\perp} - H_D^{\parallel})}, \quad (5.33)$$

where  $H_n$  is the hyperfine field,  $H_m$  is the field that restricts the domain rotation, and  $H_D^{\perp} - H_D^{\parallel}$  is the difference between the perpendicular and parallel demagnetizing fields [i.e.,  $H_D^{\perp} - H_D^{\parallel} = (D_{\perp} - D_{\parallel})M_s$ ]. (We have assumed the hyperfine field to be isotropic for simplicity.)

By analogy, for a *paramagnet*  $H_m = H_0 + (D_{\perp} - D_{\parallel})\chi H_0$  and since the transverse field is reduced by  $M/M_0$  relative to the ferromagnet, we find—if  $\chi$  is assumed to be isotropic—

$$\text{para: } \eta = (M/M_0)H_n \{H_0[1 + (D_{\perp} - D_z)\chi]\}^{-1} \\ = H_n \chi / M_0 [1 + (D_{\perp} - D_z)\chi]. \quad (5.34)$$

$\eta$  may be recognized as just the paramagnetic shift in an NMR experiment. Since at elevated temperatures and moderate fields ( $T > 50 \text{ °K}$ ;  $H_0 < 50 \text{ kOe}$ ),  $\chi/M_0 \ll 10^{-5}$ , little or no enhancement is seen for NMR in paramagnets.

For a uniaxial antiferromagnet, Eq. (5.34) is immediately applicable under the following restrictions: If  $\vec{H}_0 \parallel \hat{c}$  and  $\vec{H}_{\text{rf}} \perp \hat{c}$  and we assume for the moment that  $\chi_{\parallel} = 0$ , then

$$\text{antiferro: } \eta^{\parallel} = (H_n/M_s)\chi_{\perp}. \quad (5.35)$$

At fields  $H_0 \ll H_{\text{SF}}$ ,  $\chi_{\perp} \approx \chi_{\perp}(T_n)$  and hence the enhancement in the antiferromagnetic state is no larger than it is in the paramagnetic state at  $T = T_n$ . Alternatively one may note that  $\chi_{\perp} \approx M_s/H_E$  so that the rotation of the magnetization is restricted by the *exchange* field rather than the smaller anisotropy field, as it is in the ferromagnet. However,  $\chi_{\perp}$  increases dramatically as a function of  $\vec{H}_0 \parallel \hat{c}$  as we shall now show and may

cause  $\eta^{\parallel}$  to become appreciably larger than unity.

Since the nuclei interact with the individual electronic spin moments it is essential for the enhancement calculation to separately obtain the transverse susceptibilities  $\chi_{\perp}^{\uparrow}$  and  $\chi_{\perp}^{\downarrow}$  of the two sublattices. Using the effective field equations derived from the Hamiltonian in Eq. (1.1) one may calculate  $\chi_{\perp}^{\uparrow\downarrow}$  as a function of  $H_0$ . From the angles

$\Delta$ ,  $\theta_H$ , and  $\phi$  between the various vector quantities as indicated in Fig. 10, it is clear that, in the small-angle approximation,

$$\begin{aligned}\chi_{\perp}^{\uparrow\downarrow} &= (M_s/H_0\theta_H)(\varphi \pm \Delta); \\ \chi_{\perp} &= \chi_{\perp}^{\uparrow} + \chi_{\perp}^{\downarrow}\end{aligned}\quad (5.36)$$

with the  $+$  ( $-$ ) associated with the  $\downarrow$  ( $\uparrow$ ) sublattice magnetizations, respectively. Balancing the torques on the two sublattice results in the following two equations:

$$\begin{aligned}-H_E \sin 2\varphi + H_A \cos(\Delta - \varphi) \sin(\Delta - \varphi) + H_0 \sin(\Delta - \varphi + \theta_H) + \frac{8}{3}\pi M_s \sin\varphi \cos\varphi \\ - 2M_s D_{\perp} \sin\varphi \cos\Delta \cos(\Delta - \varphi) - 2M_s D_z \sin\varphi \sin\Delta \sin(\Delta - \varphi) = 0.\end{aligned}\quad (5.37a)$$

$$\begin{aligned}+H_E \sin 2\varphi + H_A \cos(\Delta - \varphi) \sin(\Delta - \varphi) - H_0 \sin(\pi - \Delta - \varphi - \theta_H) - \frac{8}{3}\pi M_s \sin\varphi \cos\varphi \\ + 2M_s D_{\perp} \sin\varphi \cos\Delta \cos(\Delta - \varphi) + 2M_s D_z \sin\varphi \sin\Delta \sin(\Delta - \varphi) = 0.\end{aligned}\quad (5.37b)$$

Here  $H_E = 2JZS/g\mu_B$ ,  $H_A = KS/g\mu_B$ , and we have specifically included Lorentz-field as well as demagnetizing-field corrections. Again in the small-angle approximation one finds from Eqs. (5.37a) and (5.37b),

$$\begin{aligned}\Delta &= H_0^2 \theta_H / (H_{SF}^2 - H_0^2); \\ \varphi &= H_0(\Delta + \theta_H) / 2H_E,\end{aligned}\quad (5.38)$$

where  $H_{SF}^2$  is defined in Eq. (2.3). Inserting these results for  $\Delta$  and  $\varphi$  into Eq. (5.36), we obtain

$$\chi_{\perp}^{\uparrow\downarrow} = M_s \frac{H_{SF}^2 \pm 2H_E H_0}{2H_E(H_{SF}^2 - H_0^2)} \quad (5.39)$$

and

$$\chi_{\perp} = \frac{M_s}{H_E} \frac{H_{SF}^2}{H_{SF}^2 - H_0^2}. \quad (5.40)$$

The quantities  $\chi_{\perp}^{\uparrow\downarrow}$  and  $\chi_{\perp}$  are shown in Fig. 10 as a function of  $H_{SF} - H_0$  for  $\text{MnF}_2$ . Two interesting features may be noted: (i) the separate sublattice susceptibilities increase more rapidly with increasing  $H_0$  than does  $\chi_{\perp}$  and (ii) all three quantities diverge at precisely that value of the field ( $H_0 = H_{SF}$ ) for which the energy of the  $k=0$  spin-wave mode vanishes. One may infer from the latter that the results of Eqs. (5.39) and (5.40) hold in the linear spin-wave approximation as well.

Finally, combining Eqs. (5.35) and (5.39), we obtain for the enhancements

$$\eta^{\uparrow\downarrow} = \frac{H_n}{2H_E} \frac{H_{SF}^2 \pm 2H_E H_0}{H_{SF}^2 - H_0^2} \quad (5.41)$$

with the  $+$  ( $-$ ) to be associated with  $\chi_{\perp}^{\uparrow}$  ( $\chi_{\perp}^{\downarrow}$ ), respectively.<sup>35,36</sup> In the vicinity of spin flop, Eq. (5.41) reduces to

$$\eta \approx \pm H_n / 2(H_{SF} - H_0). \quad (5.42)$$

The predicted values from Eq. (5.42) for  $^{19}\text{F}$  and

$^{55}\text{Mn}$  are compared with the rough experimental measurements in Table III. Although the agreement between experiment and theory is satisfactory for the  $^{19}\text{F}$  NMR the observed values of  $^{55}\text{Mn}$  are markedly larger than Eq. (5.42) suggests. The probable explanation for the larger  $^{55}\text{Mn}$  enhance-

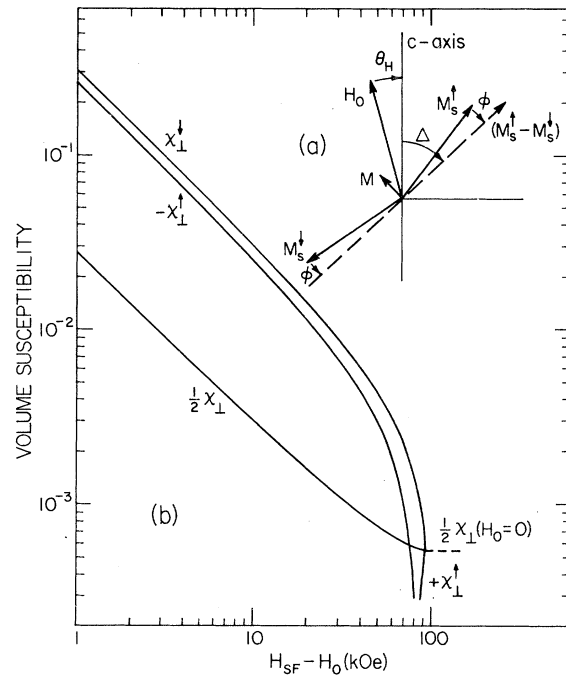


FIG. 10. Relative orientations of the sublattice magnetizations, external field, and the anisotropy axis appropriate to the calculation of the field dependence of the perpendicular susceptibilities. (a) Angles  $\theta_H$  ( $\vec{H}_0 \hat{c}$ ),  $\Delta$  ( $\vec{c} \hat{M}_s^{\uparrow} - \vec{M}_s^{\downarrow}$ ),  $\phi$  ( $\vec{M}_s^{\uparrow} \hat{M}_s^{\downarrow} - \vec{M}_s^{\downarrow}$ ) are shown. (b) Calculated sublattice ( $-\chi_{\perp}^{\downarrow}$ ,  $\chi_{\perp}^{\uparrow}$ ) and total ( $\frac{1}{2}\chi_{\perp}$ ) perpendicular susceptibilities are shown as a function of the distance from spin flop  $H_{SF} - H_0$ .

ments is that near spin flop the observed resonances have mixed electronic as well as nuclear character as a result of the larger Suhl-Nakamura interaction.<sup>16, 17</sup> This is evidenced by the fact that the predicted<sup>18</sup> frequency shift ("frequency pulling") associated with this interaction just becomes noticeable in the region close to spin flop. Since the shift  $\delta$  has the form

$$\delta \propto A^2 \langle I_z \rangle / (H_{\text{SF}} + H_0)(H_{\text{SF}} - H_0)$$

and  $^{55}\text{A} \gg ^{19}\text{A}$ , it is clear that mixed electronic and nuclear character is likely to be less important for the  $^{19}\text{F}$  NMR than it is for the  $^{55}\text{Mn}$  NMR.

## VI. CONCLUSIONS

We have used the NSLR rates of the  $^{19}\text{F}$  and  $^{55}\text{Mn}$  NMR in  $\text{MnF}_2$  to precisely test the antiferromagnetic spin-wave theory in a field region  $0 \leq H_0 < H_{\text{SF}}$ , at temperatures  $T \ll T_{\text{AE}} < T_N$ . Since the magnitude and the symmetry properties of the electron nuclear interaction for the two resonances require that two-magnon (for  $^{19}\text{F}$ ) and three-magnon (for the  $^{55}\text{Mn}$ ) scattering be the predominant mechanisms by which the respective nuclei relax, we have been able to separately compare and relate these distinct processes as a function of only one external parameter—the magnetic field. The satisfactory comparison between experiment and the predictions of low-order spin-wave scattering theory over the entire field region—except in the immediate vicinity of spin flop—confirms the validity of the thermodynamic spin-wave theory of a Heisenberg antiferromagnet. It appears to us that the difficulties that have been encountered in almost all previous NSLR studies in other antiferromagnets (e.g.,  $\text{H}^1$  in  $\text{CuCl}_2 \cdot 2\text{H}_2\text{O}$ ) in attempting to make similar comparisons represent a deficiency in the understanding and characterization of the magnon excitation spectra of more complex spin structures rather than a basic deficiency of the theory. Taken together with the research of Kaplan *et al.*,<sup>10</sup> we regard our work as a definitive study of the  $H_0$ - $T$  dependence of the thermodynamics of an antiferromagnet.

There remains a need to quantitatively understand the "critical-like" behavior of the NSLR as  $H_0$  approaches  $H_{\text{SF}}$ . Although the scattering that would involve five, seven, etc. magnons would cause increasingly rapid field dependence of the NSLR it seems unlikely that the perturbation approach would result in the simple  $(H_{\text{SF}} - H_0)^{-3/2}$  behavior that is observed for  $^{55}\text{Mn}$  ( $1/T_1$ ). Perhaps the approach taken by Turov and his collaborators for the ferromagnets in which they interpret the relaxation as a manifestation of a direct process involving the scattering of a damped magnon, would be useful to explore further in connection with the

onset of the spin-flop transition in an antiferromagnet. The difficulties implicit in their method are not inconsiderable.

It is also possible that the observed anomalous behavior of the NSLR rates in the vicinity of  $H_{\text{SF}}$  is a precursor effect signaling a dynamic instability associated with the transition to a new ground state for the electronic spin system. As such it would be unlikely that a perturbation approach which assumes small fluctuations about a well-defined "Néel" state is a proper starting point. We hope the present work will stimulate further theoretical effort in this area.

## ACKNOWLEDGMENTS

We would like to thank Dr. M. Butler for his contributions to the initial phases of this work, Dr. F. Freyne and Professor P. Pincus for discussions of the exchange enhancement problem, and Professor D. Hone and Dr. J-P. Boucher for numerous discussions and insights.

## APPENDIX A

This appendix has two purposes: first, to explore the region of validity of two model calculations of the magnon density of states  $D(E)$  and compare them with a relatively exact one. Second, we justify the assumption we have frequently used, that, at 4.2 °K, the relevant thermodynamic properties of  $\text{MnF}_2$  are dominated by the small- $\vec{k}$  region of the "thermally weighted density of states."

Both the small- $\vec{k}$  and spherical approximations<sup>37</sup> to  $E_{\vec{k}}$  as generally applied to  $\text{MnF}_2$  and  $\text{FeF}_2$  assume  $J_1 = J_3 = 0$  and result therefore in an isotropic dispersion of magnons. In the small- $\vec{k}$  approximation,

$$E_{\vec{k}}^{\pm} = E_0(2\xi_0 + 1/4 \vec{k}^2 a^2)^{1/2}, \quad (\text{A1})$$

where  $E_0 = g\mu_B H_E$ . The corresponding density of states as obtained directly from  $E_{\vec{k}}^{\pm}$  by the usual technique<sup>19</sup> is

$$D^{\pm}(E) = \frac{4VE_{\vec{k}}}{\pi^2 a^3 E_0^2} \left[ \left( \frac{E_{\vec{k}}}{E_0} \right)^2 - 2\xi_0 \right]^{1/2}. \quad (\text{A2})$$

In the spherical approximation as it was applied to the NSLR problem in<sup>37</sup>  $\text{FeF}_2$  the dispersion and density of states are

$$E_{\vec{k}}^{\text{sp}} = E_0(1 + 2\xi_0 - \cos^2 \frac{1}{2} \vec{k} \cdot \vec{r})^{1/2} \quad (\text{A3})$$

and

$$D^{\text{sp}}(E) = \frac{4V}{\pi^2 a^3} \frac{E_{\vec{k}}^{\text{sp}}}{E_0^2} \times \frac{\{\sin^{-1}[(E/E_0)^2 - 2\xi_0]^{1/2}\}^2}{[1 + 2\xi_0 - (E/E_0)^2]^{1/2} [(E/E_0)^2 - 2\xi_0]^{1/2}}, \quad (\text{A4})$$

where the dispersion extends through a spherical

zone of radius  $\vec{k}_m = \pi/a$ . Thus  $E_{\vec{k}}$  in the spherical approximation is the same as is obtained for  $\text{MnF}_2$  in the [100] direction in the first Brillouin zone.

In the long-wavelength approximation, properly formulated, there is no expectation that the zone-boundary energies or density of states should be given correctly. Therefore the model is only valid in situations where no significant thermal weighting is given to the zone-boundary magnons. If the theory is extended to temperatures for which zone-boundary magnons are important, gross underestimations of thermodynamic quantities can occur. This point apparently has not been appreciated fully in the past. The results of our calculations explicitly demonstrate this effect as shown below.

The anticipated advantage of the spherical model over the small- $\vec{k}$  approximation is that it generates a realistic peak in  $D(E)$  at an energy equal to the exact maximum spin-wave energy. This feature is shown in Fig. 11 where the two approximations are compared with a relatively exact density of states appropriate to  $\text{MnF}_2$ .

Two disadvantages of the spherical model exist in the simple form outlined here. First, the normalization is incorrect. Usually the size and shape of the Brillouin zone is chosen appropriate to the crystal structure in such a way that  $\int_{\text{BZ}} D(E) dE = N$ , where  $N$  is the total number of modes. In the spherical model, mathematical convenience dictates that one should disregard the corners of a cubic Brillouin zone which are outside of the enclosed spherical zone. In order to satisfy the normalization requirement above, Butler *et al.*<sup>37</sup> recovered the "missing" states by proportionately redistributing them over their whole zone. They used  $D(E) = (6/\pi)D^{\text{sp}}(E)$ . This has the advantage that the number of states at the zone boundary is approximately correct. Unfortunately for small energies  $D(E)$  is too large by a factor  $6/\pi$ . At low temperatures in  $\text{MnF}_2$  it is better simply to ignore the "missing" states since only the small energy density of states is important.

The second disadvantage of this model more specifically relates to  $\text{MnF}_2$ . Whereas only one peak occurs at the zone boundary in  $D^{\text{sp}}(E)$ , the exact  $D(E)$  has two peaks at slightly different energies corresponding to different directions in the real zone and is a direct consequence of  $J_1 \neq 0$ . It is important to take cognizance of this because  $D(E)$  occurs to a higher power than the first in many calculations. In the two-magnon relaxation process, for example,  $D(E)$  occurs squared. Thus, at temperatures where zone-boundary magnons are important, there is a significant difference in the calculated result if there is a single large peak in the density of states rather than two smaller

peaks. In fairness it should be pointed out that the spherical model was originally developed for  $\text{FeF}_2$  where  $J_1 \approx 0$  and there really is only a single speak in  $D(E)$ . The general conclusion for this model, then, in its applicability to  $\text{MnF}_2$ , is that it is only valid when small- $\vec{k}$  excitations are important and a suitable normalization is chosen.

Actual calculations using the three different forms of the density of states are performed by transforming the sums in  $\vec{k}$  space to numerical integrals in  $E$  space. For the two model calculations, the transformations are analytic yielding an expression, for the two-magnon case, which is a one-dimensional integral over energy. A detailed description of this procedure is given in Butler *et al.*<sup>37</sup> The necessary numerical integration was performed on a computer. Thermodynamic calculations using the exact density of states derived from Eq. (5.4) are more involved. The Brillouin zone is divided into tiny sections which are classified into constant energy surfaces;  $E(\vec{k}) = \text{constant}$ . This correspondence is then utilized by the computer to explicitly perform the sums over  $\vec{k}$  space while maintaining the restrictions imposed by the energy conserving  $\delta$  function.

In order to give a specific example of the relative behavior of the three models, we present the results of calculations of the temperature dependence of the  $^{19}\text{F}$  NSLR given by the  $(A_{yz}^1)^2$  term of Eq. (5.13). The calculation is performed for  $A_{yz}^1 = 5.4 \times 10^{-4} \text{ cm}^{-1}$  and the results are shown in Fig. 12. The NSLR temperature dependence using the exact

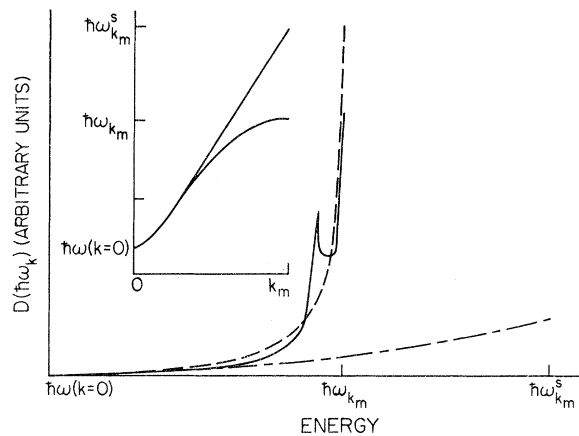


FIG. 11. Magnon dispersion and density of states in  $\text{MnF}_2$ . The insert shows the magnon energy vs  $\vec{k}$  dependence in the small- $\vec{k}$  approximation. For comparison the exact dispersion in the [100] direction is also given. The main figure compares the magnon density of states vs energy in the small- $\vec{k}$  approximations with the exact one. In order to satisfy normalization requirements, the energy in the small- $\vec{k}$  approximation must be extended to the limit  $\hbar\omega_{\vec{k}_m}^s > \hbar\omega_{\vec{k}_m}$ .

$D(E)$  was taken from the work of Kaplan *et al.*; the model calculations were performed by us. The first thing to be noticed is that all three models agree for very low temperatures  $T \ll T_N$ , but that significant disagreement occurs beginning near  $T = 6^\circ\text{K}$ . Disagreement between the three calculations at higher temperatures arises because of the form of  $D(E)$  at the zone boundary. These effects are somewhat larger for two-magnon relaxation than they might be for some other thermodynamic quantities because of the fact that the density of the states appears squared. For the spherical model  $^{19}(1/T_1)$  rises to more than an order of magnitude larger than the exact rate because of the fact that the model calculation has only a single peak at the zone boundary. In contrast, the small- $\bar{k}$  approximation rate falls far below the exact rate because of the lack of a sharp peak in  $D^s(E)$ .

It is possible to quantitatively investigate the validity of model calculations without making a direct comparison with more exact calculations. This is important because very often the exact calculations are relatively difficult to carry out. Basically, it is necessary to investigate the thermal weighting of the various parts of the Brillouin zone for the thermodynamic function of interest. For the two-magnon relaxation process, it is useful to investigate the function

$$f(T, E, H) \equiv D^2(E) \times \sin^2[\bar{k}(E) - \bar{k}(E) \cdot \frac{1}{2}(\bar{r}^I - \bar{r}^{II})] \eta^\dagger(\eta^\dagger + 1), \quad (\text{A5})$$

which is, in some sense, a "thermally weighted density of states." This function can be evaluated according to whatever mathematical model is convenient. A calculation can be considered to be valid as long as there is a significant amplitude of  $f(T, E, H)$  only in regions of the Brillouin zone for which  $D(E)$  is correctly described. Shown in Fig. 13 are plots of  $f(T, E, H)$  calculated in the small- $\bar{k}$  approximation for two temperatures and extremes of magnetic field. The curves are all scaled for simple comparison; the relative amplitude between curves is not meaningful. It is clear that for temperatures as high as  $4.2^\circ\text{K}$  all contributions to the NSLR arise from the small- $\bar{k}$  region. Because of the fact that the peak in  $f(T, E, H)$  does not shift significantly as a function of  $H_0$  it is even possible to describe the field dependence of the two-magnon NSLR in  $\text{MnF}_2$  in terms of an Einstein distribution with an energy  $E^*$  (or  $\bar{k}^*$ ) defined by the position of this peak. At only slightly higher temperatures the states near the zone-boundary energy  $\hbar\omega_{\bar{k}_m}$  become important, as is shown in Fig. 13 for  $T = 8.2^\circ\text{K}$ . It should be noticed, incidentally, that just below  $8.2^\circ\text{K}$  is the region in which there begins to be a significant deviation of the model calculations of the  $^{19}\text{F}$  NSLR from the exact rate as shown in Fig. 12. It is thus clear that details of the density of states at the zone boundary can become important at surprisingly low temperatures so that great care must be exercised in interpreting calculations which

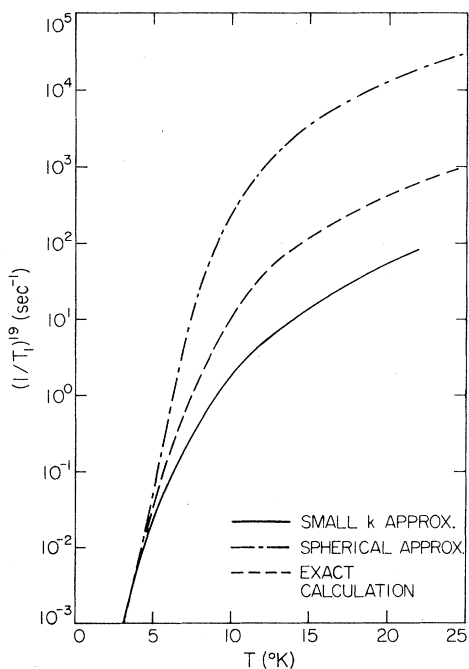


FIG. 12. Comparison of two model calculations of the  $^{19}\text{F}$  NMR relaxation in  $\text{MnF}_2$  with the results of the exact calculation at  $H_0 = 0$  as a function of temperature.

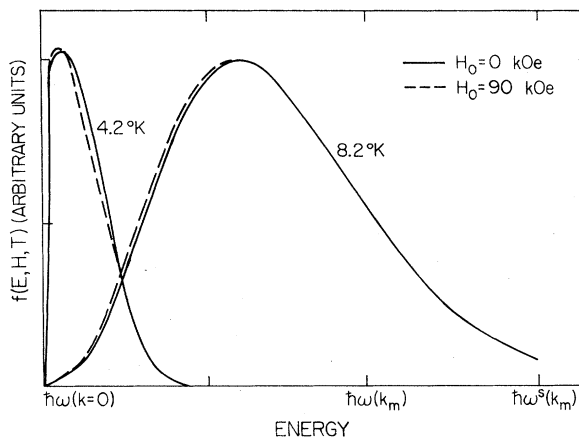


FIG. 13. Comparison of the normalized "thermally weighted two-magnon density of states," as is appropriate to the  $^{19}\text{F}$  nuclear magnetic relaxation in  $\text{MnF}_2$ , at two temperatures and extremes of external fields.

utilize approximate dispersion relations which are good only for small  $\vec{k}$ .

Historically most spin-wave NSLR calculations have made use of the small- $\vec{k}$  approximation to the density of states. This was originally used by Moriya<sup>26</sup> and Van Kranendonk and Bloom<sup>38</sup> and more recently Lowe and Whitson.<sup>39</sup> In the first two cases, the agreement of the experiment with theory was quite poor for reasons which were not understood. In the third case agreement was obtainable by invoking three-magnon relaxation processes in addition to two-magnon ones. We would like to point out, however, that in contrast with the present work in  $\text{MnF}_2$ , the temperatures at which the NSLR data were taken ( $T \approx \frac{1}{4} T_N$ ) in  $\text{CuCl}_2 \cdot 2\text{H}_2\text{O}$  and similar compounds are such that one would not expect the small- $\vec{k}$  approximation to be applicable. In support of this argument it should be noticed that the qualitative difference in Fig. 12 between  $^{19}\text{F}$  calculated in the small- $\vec{k}$  approximation and the more exact calculation is very much the same as the difference between previous two-magnon calculations<sup>26,38,39</sup> and the  $\text{CuCl}_2 \cdot 2\text{H}_2\text{O}$  NSLR data.

#### APPENDIX B

One of the most important differences in the NSLR of  $^{55}\text{Mn}$  and  $^{19}\text{F}$  nuclei in  $\text{MnF}_2$  is that the relaxation of the former arises overwhelmingly from fluctuations of the spin on the same site, whereas that of the latter arises from the constructive or destructive interference between the fluctuating spins at the three neighboring sites. We have already shown that at 4.2 °K for the  $^{19}\text{F}$  nuclei, destructive interference plays an important role in explaining why the  $^{19}\text{F}$  NSLR rate is as small as it is with respect to the  $^{55}\text{Mn}$  NSLR rate near spin flop. It is useful, therefore, to investigate experimentally to what extent site symmetry is important in the mechanisms which give rise to the anomalous peak in the  $^{19}\text{F}$  relaxation.

It was suggested<sup>40</sup> that specific information concerning the  $^{19}\text{F}$  site symmetry could be obtained by investigating the NSLR of those nuclei which were near neighbors to a nonmagnetic  $\text{Zn}^{2+}$  impurity in  $\text{MnF}_2$ .

It was previously demonstrated<sup>15</sup> that the substitution for  $\text{Mn}^{2+}$  of 1-at. %  $\text{Zn}^{2+}$  as an impurity in  $\text{MnF}_2$  had little effect on the NSLR of  $^{19}\text{F}$  nuclei which were not immediate neighbors to the impurity. In addition it was shown that  $1/T_1$  for the  $^{19}\text{F}$  resonance associated with a  $\text{Zn}^{2+}$  impurity at a type-II site was only increased by a factor of 2. Thus the  $^{19}\text{F}$  "type-II" impurity-associated resonance effectively has had the type-II  $\text{Mn}^{2+}$  spin removed and hence it is possible to investigate fluctuations which are due to the type-I  $\text{Mn}^{2+}$  spins

alone. Therefore  $^{19}\text{F}$  NSLR measurements were made near  $H_D$  for  $\text{F}^-$  sites of this type. Near  $H_D$  the  $\text{MnF}_2:\text{Zn}$  type-II resonance branches occur in the region of 120 and 615 MHz.

NSLR data taken on the downgoing branch of the  $^{19}\text{F}$  type-II resonance near spin flop in  $\text{MnF}_2:\text{Zn}$  (1 at. %) are shown in Fig. 14. (Because of decreased sensitivity in the UHF range, measurements were made only on the downgoing branch. A search for the corresponding type-I  $\text{MnF}_2:\text{Zn}$  resonance was not made, and it had not been previously observed.) The sharp increase in the NSLR of this impurity related resonance in the same range over which the similar increase is observed in pure  $\text{MnF}_2$  gives a qualitative indication that the anomalous increase in the relaxation rate does not depend upon the presence of the type-II electronic spin.

A very rough interpolation in Fig. 14 between our data points at  $H_0 = 80$  kOe and the data of Butler *et al.*<sup>15</sup> at  $H_0 = 0$  for  $^{19}\text{F}$  show quite clearly that even below the anomalous region the magnetic field dependence of this rate is much stronger than it is for  $^{19}\text{F}$  in pure  $\text{MnF}_2$ . This feature indicates that the removal of a type-II  $\text{Mn}^{2+}$  spin eliminates the possibility of destructive interference taking place at the  $^{19}\text{F}$  sites in the three-magnon relaxation processes. It was this inter-

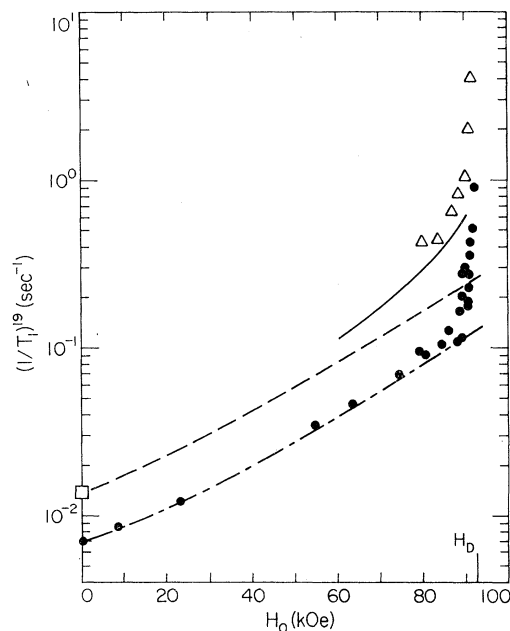


FIG. 14. Comparison of experiment with theory for  $^{19}\text{F}$  for the impurity-associated  $^{19}\text{F}$  Zn-II resonance in  $\text{MnF}_2:\text{Zn}$  (1 at. %) at 4.2 °K as a function of magnetic field; the triangles are our data whereas the square point is that of Ref. 15. The solid dots are the points for the corresponding resonance in pure  $\text{MnF}_2$ , as is also shown in Fig. 3.

ference that made the latter processes unimportant at the  $^{19}\text{F}$  site in pure  $\text{MnF}_2$ .

We interpret the above experimental results in terms of the two- and three-magnon NSLR theories adapted in such a way as to take the  $\text{Zn}^{2+}$  (missing  $\text{Mn}^{2+}$  spin) impurity into account. Assuming that there are no changes in local spin orientation, there are two physical effects which change the relaxation rate at the impurity associated  $^{19}\text{F}$  site. First, the local excitation spectrum is relatively "soft."<sup>41</sup> This means that lower-energy magnons are more likely to generate a spin deviation at a site near a  $\text{Zn}^{2+}$  impurity than they are at a site far from one. This arises from the fact that the next-nearest  $\text{Mn}^{2+}$  neighbors to the spinless  $\text{Zn}^{2+}$  impurity have only seven instead of the usual eight exchange couplings. This "soft" impurity-mode spectrum was invoked by Butler *et al.*<sup>15</sup> to explain the fact that at  $H_0 = 0$  the impurity-related nuclei had a faster relaxation rate than the other ones, i.e.,  $^{19}(1/T_1)_{\text{Zn-II}} = 2[^{19}(1/T_1)_{\text{pure}}]$ . Second, because of the fact that all negative contributions to the cancellation of transverse fluctuations in odd-magnon processes at the  $^{19}\text{F}$  sites arise from the type-II electronic spin, these cancellation effects cannot exist at the  $^{19}\text{F}$  Zn-II site.

Using the phenomenological approach developed in Sec. V it is possible to estimate the relative magnitudes of  $^{19}(1/T_1)_{\text{Zn-II}}$  and  $^{55}(1/T_1)_{\text{nnn}}$  at the corresponding type-I sites. For this case, explicitly excluding type-II spins, we rewrite Eq. (5.23) as

$$^{19}(1/T_1)_{\downarrow\text{Zn-II}} = 2A_{\uparrow}^2 \tilde{S}_{\downarrow}^a (1 + \eta) \approx 4A_{\uparrow}^2 \tilde{S}_{\downarrow}^a. \quad (\text{B1})$$

Here  $\tilde{S}_{\downarrow}^a$  is the enhanced fluctuation amplitude of the next-near-neighbor  $\text{Mn}^{2+}$  spins to the  $\text{Zn}^{2+}$  impurity site. The ratio of the  $^{55}\text{Mn}$  to  $^{19}\text{F}$  relaxation rates will be

$$R_{\downarrow} = \frac{^{19}(1/T_1)_{\downarrow\text{Zn-II}}}{^{55}(1/T_1)_{\uparrow\text{nnn}}} = \frac{A_{\uparrow}^2}{A_{55}^2} = \frac{1}{12}.$$

Clearly in this case the exclusion of interference in the transverse fluctuations at the  $^{19}\text{F}$  Zn-II site leads to a smaller difference between the  $^{19}\text{F}$  and corresponding  $^{55}\text{Mn}$  relaxation rates than is the case in the pure crystal. Thus the "three-magnon" relaxation would be expected to have the same order of magnitude as the two-magnon rate well below the anomalous region in  $^{19}(1/T_1)_{\downarrow\text{Zn-II}}$ . It is instructive, therefore, to attempt to scale the calculation of the  $^{55}\text{Mn}$  three-magnon NSLR for the pure crystal to the case of the neighbors to the  $\text{Zn}^{2+}$  impurity.

In order to scale the  $^{55}\text{Mn}$  NSLR in the pure material to the  $^{19}\text{F}$  Zn-II NSLR several assumptions are necessary. First, we assume that the

"soft" local-magnon spectrum can be described by a "reduced spectral weight"<sup>41</sup>  $A_i(E)$ . This spectral weight serves to redefine the density of states appropriate to the  $\text{Mn}^{2+}$  nnn to the  $\text{Zn}^{2+}$  impurity. Specifically the density of states for the impurity modes is given by  $D_i(E) = A_i(E) D(E)$ . Second, as shown in Appendix A, the NSLR is dominated by a peak at low energy in the "thermally weighted density of states" whose position  $E^*$  is independent of  $H_0$ . Therefore it is possible to describe the  $H_0$  dependence of  $^{19}(1/T_1)$  and  $^{55}(1/T_1)$  qualitatively in terms of an Einstein distribution with an energy  $E^*$ . Third, we assume that at  $H_0 = 0$ ,  $^{19}(1/T_1)_{\text{Zn-II}}$  arises primarily from two-magnon processes. Then from the data at  $H_0 = 0$  we can write

$$\frac{^{19}(1/T_1)_{\text{Zn-II}}}{^{19}(1/T_1)_{\text{pure}}} = \frac{A_i^2(E^*) D^2(E^*)}{D^2(E^*)} = 2$$

or

$$A_i(E^*) = \sqrt{2}.$$

Here we have made use of the fact that the two-magnon relaxation rate is proportional to the square of the density of states. Three magnon relaxation is proportional to  $D(E) D(E') D(E'')$ , where  $E$ ,  $E'$ , and  $E''$  represent the energies of the three magnons. Then near spin-flop where the magnon gap is small, the energy-conserving  $\delta$  function will allow all three magnons to be characterized by the energy at the peak of the "thermally weighted density of states." Finally we scale the impurity relaxation according to the formula

$$\begin{aligned} ^{19}\left(\frac{1}{T_1}\right)_{\downarrow\text{Zn-II}} &= \frac{A_{\uparrow}^2}{A_{55}^2} A_i^3(E^*) ^{55}\left(\frac{1}{T_1}\right)_{\uparrow 3 \text{ magnon}} + 2 ^{19}\left(\frac{1}{T_1}\right)_{\downarrow 2 \text{ magnon}} \\ &= 2^{3/2} \frac{A_{\uparrow}^2}{A_{55}^2} ^{55}\left(\frac{1}{T_1}\right)_{\uparrow 3 \text{ magnon}} + 2 ^{19}\left(\frac{1}{T_1}\right)_{\downarrow 2 \text{ magnon}}. \end{aligned}$$

The expression  $^{55}(1/T_1)_{\uparrow 3 \text{ magnon}}$  as a function of  $H_0$  is taken from the calculations of Freyne and Pincus reduced by a factor of  $\frac{1}{2}$  for the reasons discussed in Sec. VB in interpreting the results of our  $^{55}\text{Mn}$  NSLR measurements. The result of this scaling procedure is shown in Fig. 14 with the  $^{19}\text{F}$  Zn-II data. It can be seen that the major part of the upturn in the relaxation rate which occurs below the anomalous peak in this impurity-related  $^{19}\text{F}$  NSLR can be explained in terms of the two- and three-magnon relaxation processes. Again we emphasize the point that the reason the three-magnon processes are important here is that cancellation of field fluctuations cannot occur when a spinless impurity occupies the type-II site.

- \*Present address: Department of Physics, University of Utah, Salt Lake City, Utah 84112.
- †Work supported in part by the National Science Foundation.
- <sup>1</sup>F. Keffer, *Handbuch der Physik* (Springer-Verlag, Berlin, 1965), Vol. XVIII, Pt. 2, p. 1.
- <sup>2</sup>A. Okazaki, K. C. Turberfield, and R. W. H. Stevenson, *Phys. Lett.* **8**, 9 (1964).
- <sup>3</sup>C. Trapp and J. W. Stout, *Phys. Rev. Lett.* **10**, 157 (1963).
- <sup>4</sup>G. G. Low, *Proc. Phys. Soc. Lond.* **82**, 992 (1963).
- <sup>5</sup>V. Jaccarino and L. R. Walker, *J. Phys. Radium* **20**, 341 (1959).
- <sup>6</sup>J. W. Stout and H. Adams, *J. Am. Chem. Soc.* **64**, 1535 (1942).
- <sup>7</sup>F. M. Johnson and A. H. Nethercott, *Phys. Rev.* **114**, 705 (1959).
- <sup>8</sup>J. P. Kotthaus and V. Jaccarino, *AIP Conf. Proc.* **10**, 57 (1972).
- <sup>9</sup>Y. Shapira and S. Foner, *Phys. Rev. B* **1**, 3083 (1970).
- <sup>10</sup>N. Kaplan, R. Loudon, V. Jaccarino, H. J. Guggenheim, D. Beeman, and P. A. Pincus, *Phys. Rev. Lett.* **17**, 357 (1966).
- <sup>11</sup>A. R. King and D. Paquette, *Phys. Rev. Lett.* **30**, 662 (1973).
- <sup>12</sup>For a general review of NMR in antiferromagnets, see V. Jaccarino, in *Magnetism*, edited by G. T. Rado and H. Suhl (Academic, New York, 1965), Vol. 2A, Chap. 5.
- <sup>13</sup>H. Yasuoka, Tin Ngwe, V. Jaccarino, and H. J. Guggenheim, *Phys. Rev.* **177**, 667 (1969).
- <sup>14</sup>A. M. Clogston, J. P. Gordon, V. Jaccarino, M. Peter, and L. R. Walker, *Phys. Rev.* **117**, 1222 (1960).
- <sup>15</sup>M. Butler, V. Jaccarino, N. Kaplan, and H. J. Guggenheim, *Phys. Rev. B* **1**, 3058 (1970).
- <sup>16</sup>H. Suhl, *Phys. Rev.* **109**, 606 (1958).
- <sup>17</sup>T. Nakamura, *Prog. Theor. Phys.* **20**, 542 (1958).
- <sup>18</sup>P. G. De Gennes, P. A. Pincus, F. Hartmann-Boutron, and J. M. Winter, *Phys. Rev.* **129**, 1105 (1963).
- <sup>19</sup>C. Kittel, *Quantum Theory of Solids* (Wiley, New York, 1967).
- <sup>20</sup>T. Holstein and H. Primakov, *Phys. Rev.* **58**, 1098 (1940).
- <sup>21</sup>It has sometimes been stated that the hyperfine interaction must be anisotropic for the two-magnon process to be allowed. This is incorrect. A *diagonal* anisotropic hyperfine interaction will *not* allow Raman scattering.
- <sup>22</sup>P. Pincus, *Phys. Rev. Lett.* **16**, 398 (1966); D. Beeman and P. Pincus, *Phys. Rev.* **166**, 359 (1968).
- <sup>23</sup>F. Freyne and P. Pincus (unpublished).
- <sup>24</sup>A. Brooks Harris, *J. Phys. C* **2**, 469 (1969).
- <sup>25</sup>A. Brooks Harris, *Phys. Rev.* **183**, 486 (1969).
- <sup>26</sup>T. Moriya, *Prog. Theor. Phys.* **16**, 23 (1956); **16**, 641 (1956).
- <sup>27</sup>In the Green's-function approach of Ref. 24, where the  $\langle TS_R^+(t)S_R^-(t') \rangle$  spin Green's function was expressed in terms of the boson Green's functions  $\langle Ta_R(t)a_R^\dagger(t') \rangle$  and  $\langle Ta_R^\dagger(t)a_R(t') \rangle$  for calculating the transverse fluctuations that led to nuclear relaxation in the ferromagnet, one would now have to calculate  $\langle Ta_R^\dagger(t)a_R(t')a_R^\dagger(t')a_R(t) \rangle$  corresponding to  $\langle TS_z(t)S_z(t') \rangle$ . The notation is that of Ref. 24.
- <sup>28</sup>F. Freyne, Ph.D. thesis (UCLA, 1973) (unpublished).
- <sup>29</sup>E. A. Turov and M. P. Petrov, *Nuclear Magnetic Resonance in Ferro- and Antiferromagnets* (Halsted, New York, 1972). References to original papers by Turov and collaborators are given therein.
- <sup>30</sup>An ambiguity arises because there is not a one-to-one correspondence in the Green's-functions calculations and perturbation calculations as to what is meant by the words "one-magnon" process.
- <sup>31</sup>H. Yamazaki, *J. Phys. Soc. Jpn.* **32**, 5 (1972).
- <sup>32</sup>J. P. Kotthaus and V. Jaccarino, *Phys. Lett.* **A42**, 361 (1973).
- <sup>33</sup>A. C. Gossard and A. M. Portis, *Phys. Rev. Lett.* **3**, 164 (1959).
- <sup>34</sup>C. H. Cobb, V. Jaccarino, M. A. Butler, J. P. Remeika, and H. Yasuoka, *Phys. Rev. B* **7**, 307 (1973).
- <sup>35</sup>A very interesting effect is predicted (and is observed) by Eq. (5.41) for the <sup>55</sup>Mn NMR. Since <sup>55</sup>H<sub>n</sub> < 0 one finds  $\eta^\dagger = -1$  when  $H_0 \approx 4.5$  kOe in which case  $H_{\text{eff}} = 1 + \eta = 0!$  In a field scan from 5 to 15 kOe at 680 MHz on the <sup>55</sup>ν<sub>4</sub> branch the quadrupolar components of the <sup>55</sup>Mn NMR were appreciably smaller at the low field than they were at the higher ones.
- <sup>36</sup>A. R. King, D. Paquette, and V. Jaccarino, *Phys. Lett.* (to be published).
- <sup>37</sup>M. Butler, Tin Ngwe, N. Kaplan, and H. J. Guggenheim, *Phys. Rev.* **184**, 365 (1969).
- <sup>38</sup>J. Van Kranendonk and M. Bloom, *Physica* **22**, 545 (1956); A. Mitchell, *J. Chem. Phys.* **27**, 59 (1957).
- <sup>39</sup>I. J. Lowe and D. W. Whitson, *Phys. Rev. B* **6**, 3262 (1972).
- <sup>40</sup>P. Pincus (private communication).
- <sup>41</sup>L. R. Walker, B. C. Chambers, D. Hone, and H. Callen, *Phys. Rev. B* **5**, 1144 (1972).